

國立交通大學

電信工程學系

碩士論文

利用頻率選擇面設計雙頻可切換

場型之波束天線



Novel Dual-Band Pattern Reconfigurable Reflector
Antennas Using Switching Frequency Selective
Surfaces

研究生：柯智祥 (Chih-Hsiang Ko)

指導教授：鍾世忠 教授 (Dr. Shyh-Jong Chung)

中華民國九十七年九月

利用頻率選擇面設計雙頻可切換場型之波束天線

Novel Dual-band Pattern Reconfigurable Reflector Antennas Using Switching Frequency Selective Surfaces

研究生：柯智祥

Student : Chih-Hsiang Ko

指導教授：鍾世忠 博士

Advisor : Dr. Shyh-Jong Chung

國立交通大學

電信工程學系

碩士論文



Submitted to Department of Communication Engineering

College of Electrical and Computer Engineering

National Chiao Tung University

in Partial Fulfillment of the Requirements

For the Degree of Master of Science

In Communication Engineering

September 2008

Hsinchu, Taiwan, Republic of China

中華民國九十七年九月

利用頻率選擇面設計雙頻可切換場型之波束天線

研究生：柯智祥 指導教授：鍾世忠 博士

國立交通大學電信學系

碩士論文

摘要

隨著無線通訊的發展，有限的頻寬不斷地被數量眾多的無線通訊設備使用及分割，因此，如何有效地使用通訊頻寬並將其他干擾減至最低將是目前無線通訊設備在設計上一個重要的課題。可變換場型並集中能量的智慧型天線是一個解決此問題的好選擇。

在本論文中，我們提出一種新型的雙頻的智慧型天線。利用可改變特性的頻率選擇平面當做主要的反射面架構，並配合直角反射面天線的運作原理及電路開關的狀態，設計出三個雙頻的智慧型天線，可使用於 2.45 GHz 及 5.25 GHz 的頻段中。藉由各面上開關的組合，此天線可以包括許多不同的場型。

第一個天線的反射面只能運作在某一個頻率，因此，對於雙頻的智慧型天線來說，雙層的反射面設計是必需的，同時也增加了使用體積；而第二個天線的設計中，將單一反射面設計成可操作在雙頻，如此可減少天線體積，並可減少開關的使用數量；在第三個天線中，一種更為簡單的雙頻反射面架構被提出，在每一邊僅用一個長方形的環形共振器，如此可更加簡化天線的複雜度及開關的設計。而在實際的應用當中，全向性場型跟單一方向性場型的切換是最重要的，因此在以上的設計中，我們主要專注研究在此兩種場型的特性與切換。

Novel Dual-band Pattern Reconfigurable Reflector Antennas Using Switching Frequency Selective Surfaces

Student : Chih-Hsiang Ko Advisor : Dr. Shyh-Jong Chung

Department of Communication Engineering
National Chiao Tung University

ABSTRACT

With the development of the wireless communication, more and more devices share the limited bandwidth for communication. Therefore, how to reduce the interference from other devices and environment and use the limited bandwidth efficiently is one of the important subjects. A smart antenna which can change radiation patterns and focus the patterns is a good candidate to solve those problems.

In this thesis, a novel dual-band smart antenna is developed. By the switching frequency selective surface, the principle of a right angle corner reflector antenna, and the operation of switches, three dual-band pattern reconfigurable antennas are investigated. The operating frequencies in our design are 2.45 GHz and 5.25 GHz. Through combinations of switches on reflecting walls, multiple radiation patterns can be obtained.

Each reflecting wall of the first proposed pattern reconfigurable antenna operates only at one frequency; therefore, Two-layer reflecting walls are needed here. However, the volume of the completed antenna is about one-wavelength of 2.45 GHz square due to the principle of the corner reflector antenna. In the second proposed antenna, a reflecting wall can operate at two frequencies. As a result, the size of the antenna can be reduced, and the amount of switches can be decreased too. Finally, a dual-band pattern reconfigurable antenna with a simpler structure such as a rectangular loop is developed without the damages to the original properties belonging to the second antenna. Since omni-directional and directional patterns are the most important in application, we mostly focus on those two patterns in our design.

Acknowledgement

在這篇碩士論文完成的同時，我首先要感謝的就是我的指導教授鍾世忠博士。我從專題開始就跟著鍾世忠教授做一些天線方面的研究，雖然一開始有很多不懂的地方，但是教授他總是會適時地給予指導，讓我可以了解到天線的原理及設計方法；此外，教授也一直鼓勵我要多看期刊論文，以增加自己的專業知識跟想法，這對我來說助益是很大的，讓我在短時間內，對於天線的觀念建立起來，使我可以盡早做研究而順利畢業。因此，真的由衷感謝鍾世忠教授這三年來的指導。

而譚怡揚學長是我另一個要感謝的人，這篇論文的完成，多虧有學長的啟發跟討論，讓我了解「頻率選擇面」的原理跟設計想法，而學長做的單頻的場型可偏天線也是本論文的前身，因此學長的幫忙真是不言而喻啊！

當然囉！在我們前瞻實驗室中，大家都給了我很多的幫助。什麼都懂的王侑信學長，在我對於天線觀念及論文不懂的地方，都可以給予教學，讓我突破盲點，我天線知識的建立他也是功臣之一呢！凌菁偉學姊是算是一開始我最早認識的吧！她從專題生開始就帶著我們專題生，了解研究生是怎麼做事的；而當我進來實驗室之後，她也一直很照顧著大家，幫了大家很多的忙，可謂是實驗室之「母」啊！再來就是林靖凱學長啦！他是最愛跟他爭論東西的人了，不過也因為可以跟他爭論一些概念，讓我對一些東西有了不一樣的觀點，而他也會用手把東西算出來，當初跟他一起把期中期末考古題打敗的經驗還真是有趣呢！天線組的最後一個學長—莊肇堂，雖然跟他只認識一年，不過他可是濾波器專門的呢！雷達組的兩位學長：何丹雄跟林明達學長，可是很辛苦的兩位呢！常常看到他們在為了雷達的事用到很晚，真是辛苦了！


而不知道該是算跟我同屆還是學長的碩二同學們，真的很開心可以跟你們一起畢業。超級愛吹噓的蘇邵軒，最後變成我的好車友；聽說之前是系排隊長的王思本，在實驗室是個宅宅，但是他也是神手本，沒有他調不出來的天線呢；洪傳恩則是最讓我判若兩人的人，他曾經在我腦中是的正直的少年，沒想到認識他以後，才知道他一點都不正直，不過，也因為這樣，實驗室多了很多八卦跟樂趣呢！他是我的好車友啊！而要跟我去騎車環島的馬義翔更是不能不提啊，他可是我畢業後的同行者

啊！我的天線也因為有他的幫助，讓我可以及時趕出來，去量測，真是很謝謝他。再來，電腦通黃天建學長，他真的是無所不能，只要有什麼電腦的問題，問他就對了啦！而 IC 組的清標學長真的是長不大，雖然跟他沒什麼研究上的交集，不過跟他聊天還蠻有趣的呢！感覺是好好人的佩宗，常常看到他一個人在焊電路，真是苦命啊！

再來，就是理論上跟我同屆的三位啦！許少華，號稱許董，是真性情男子，也因為他相信「實驗室沒有秘密」，而讓他對實驗室真的沒有秘密；賴浩宇，俗稱浩呆，這個名稱的理由，我想大家都懂了，不過，他真的是一個好好人的超宅宅；池冠儀，同位語：小池，她是實驗室的幽靈人物，真的超少來的，最常跟他說的話大概是「快來丟垃圾吧！」，但是她到羽球場上，可是一名猛將呢！

實驗室助理，陳珮華，外號一堆，每個人都叫他不一樣的名字。不過，實驗室有她真的讓我們少了很多麻煩，雖然他桌上真的超亂，但是她總是可以找到那些東西，真是太神奇了。而在前幾個月，她也結婚了，就祝她快生吧！XDDDD

真的很開心我可以加入這個前膽微波實驗室（我還是習慣叫「Lab912」），讓我可以很開心地渡過專題跟研究生的這兩年。



謝謝大家啦！

CONTENTS

摘要.....	I
ABSTRACT.....	II
ACKNOWLEDGEMENT.....	III
CONTENTS.....	V
CONTENTS OF TABLES.....	VII
CONTENTS OF FIGURES	VIII
CHAPTER 1 INTRODUCTION	1
CHAPTER 2 THEORY OF THEORY OF CORNER REFLECTOR ANTENNA AND FREQUENCY SELECTIVE SURFACE.....	7
2-1 CORNER REFLECTOR ANTENNA.....	7
2-2 FREQUENCY SELECTIVE SURFACE	11
CHAPTER 3 DUAL-BAND PATTERN RECONFIGURABLE ANTENNA WITH TWO-LAYER WALLS	13
3-1 ANTENNA CONFIGURATION.....	13
3-2 DESIGN OF RECONFIGURABLE FSS STRUCTURES	15
3-3 DESIGN OF THE DUAL-BAND PATTERN RECONFIGURABLE REFLECTOR ANTENNA WITH TWO-LAYER WALLS	23
3-3-1 Functions of the two more half rectangular loops printed on the inner wall	23
3-3-2 Interactions between the inner walls and the feeding antenna	24
3-3-3 Design of the feeding antenna	25
3-4 MEASUREMENT RESULTS	28
CHAPTER 4 DUAL-BAND PATTERN RECONFIGURABLE ANTENNA WITH SINGLE-LAYER WALLS	33
4-1 ANTENNA CONFIGURATION.....	33
4-2 DESIGN PROCEDURE OF THE DUAL-BAND FSS WALLS	35
4-2-1 Spacing between the wall and the feeding antenna	35
4-2-2 Switching dual-band FSS elements	37
4-2-3 Design of the feeding antenna	45
4-3 MEASUREMENT RESULTS	47

CHAPTER 5 DUAL-BAND PATTERN RECONFIGURABLE ANTENNA BY FOUR SWITCHING RECTANGULAR LOOPS..... 52

5-1 ANTENNA CONFIGURATION..... 52

5-2 DESIGN OF DUAL-BAND PATTERN RECONFIGURABLE STRUCTURES WITH A SINGLE LOOP 54

5-2-1 Design of the reflector by a single loop54

5-2-2 Design of the feeding antenna59

5-3 MEASUREMENT RESULTS 61

CHAPTER 6 CONCLUSION..... 66

REFERENCES..... 67



CONTENTS OF TABLES

TABLE I THE IEEE STANDARDS OF 802.11 A/B/G/N..... 1

TABLE II THE DEFINITIONS OF THE TWO FUNDAMENTAL CASES AND THE SIMULATED AND MEASURED RESULTS OF THE DUAL-BAND PATTERN RECONFIGURABLE ANTENNA WITH TWO-LAYER WALLS..... 29

TABLE III THE DEFINITIONS OF THE TWO FUNDAMENTAL CASES AND THE SIMULATED AND MEASURED RESULTS OF THE DUAL-BAND PATTERN RECONFIGURABLE ANTENNA WITH SINGLE-LAYER WALLS..... 48

TABLE IV THE DEFINITIONS OF THE TWO FUNDAMENTAL CASES AND THE SIMULATED RESULTS OF THE DUAL-BAND PATTERN RECONFIGURABLE ANTENNA BY FOUR RECTANGULAR LOOPS 62



CONTENTS OF FIGURES

Fig. 1.1. Geometry of a 2-D pattern reconfigurable antenna based on Yagi-Uda antennas.	3
Fig. 1.2. Geometry of a 3-D pattern reconfigurable antenna based on Yagi-Uda antennas.	4
Fig. 1.3. Geometry of a 3-D pattern reconfigurable antenna by changing feeding locations	4
Fig. 1.4. Geometry of a 3-D pattern reconfigurable antenna with circle arrangement of parasitic elements.	5
Fig. 1.5. A pattern diversity antenna by changing the induced current distribution on parasitic elements.	5
Fig. 2.1. The configuration of a corner reflector antenna.	7
Fig. 2.2. The corner reflector with images shown and how they account for reflections... 8	8
Fig. 2.3. Principal plane patterns, $ AF $, for a right angle corner reflector.	8
Fig. 2.4. Geometry of a three-dimensional corner reflector antenna.	9
Fig. 2.5. Geometry of a triple corner reflector antenna.	9
Fig. 2.6. Geometry of a corner reflector antenna with the cylindrical corner.....	10
Fig. 2.7. Geometry of a pattern reconfigurable antenna evolved from Yagi-Uda antennas and corner reflector antennas.	10
Fig. 2.8. (a) An electron in filter plane undergoes oscillations driven by source wave. (b) An electron constrained to move along wire cannot undergo oscillations.....	11
Fig. 2.9. Different shapes of the FSS structures.	12
Fig. 3.1. Configuration of the proposed dual-band pattern reconfigurable antenna.	13
Fig. 3.2. Geometries of the dual-band FSS structures (a) the outer walls (b) the inner walls	15
Fig. 3.3. Current distributions of the FSS structures at 2.45 GHz on (a) two rectangular loops. (b) a switching FSS when the switch is on. (c) a switching FSS when the switch is off.	17

Fig. 3.4. Current distributions of the FSS structures at 5.25 GHz on (a) two rectangular loops. (b) a switchable FSS when the switch is on. (c) a switchable FSS when the switch is off.	18
Fig. 3.5. The simulation model for designing FSS structures.....	19
Fig. 3.6. The simulated transmission coefficients at (a) 2.45 GHz (b) 5.25 GHz when the switches are in ON-state or Off-state.	20
Fig. 3.7. The simulated current distributions in the dual-band pattern reconfigurable reflector antenna at 2.45 GHz (large loops) and 5.25 GHz (small loops) in (a) ON-state. (b) Off-state.....	21
Fig. 3.8. The comparison of the patterns in $\phi = 45^\circ$ plane in case 2 at 5.25 GHz between the FSS wall for 5.25 GHz with corner rings and without corner loops.	24
Fig. 3.9. The comparison of the patterns in $\phi = 45^\circ$ plane in case 2 at 2.45 GHz between the switches, S_{1b} & S_{4b} , in off-state and on-state.....	25
Fig. 3.10. The dual-band feeding antenna with two trident structures.	26
Fig. 3.11. The measured and simulated return loss of the dual-band feeding antenna.	27
Fig. 3.12. The photo of the complete dual-band pattern reconfigurable reflector antenna.	28
Fig. 3.13. The measured and simulated patterns of Case 2 at (a) 2.45 GHz (b) 5.25 GHz.	30
Fig. 3.14. The measured and simulated patterns of Case 1 at (a) 2.45 GHz (b) 5.25 GHz.	31
Fig. 4.1. The configuration of the proposed dual-band pattern reconfigurable antenna...	33
Fig. 4.2. The configuration of the proposed dual-band pattern reconfigurable antenna...	35
Fig. 4.3. The pattern variations for various spacing, d , (a) at 2.45 GHz (b) at 5.25 GHz.	36
Fig. 4.4. The geometry of the switchable dual-band frequency selective surface.	37
Fig. 4.5. The induced current distribution on the reflecting loops (a) at 2.45 GHz. (b) at 5.25 GHz. (c) at 2.45 GHz (d) at 5.25 GHz when the switch is impassable. (e) at 2.45 GHz (f) at 5.25 GHz when the switch is passable.....	38
Fig. 4.6. The simulation model for designing dual-band switchable FSS structures.....	39
Fig. 4.7. The transmission coefficient curves of the reflectors for various heights of (a) the center loop (b) two side loops.	40

Fig. 4.8. The transmission coefficient curves of the reflectors for various thickness of (a) the center loop (b) two side loops.	41
Fig. 4.9. The transmission coefficient curves of the reflectors for various horizontal position respect to the center point of the wall of two side loops.	42
Fig. 4.10. The transmission coefficient of the proposed reflector in ON-state and Off-state.	42
Fig. 4.11. The simulated current distribution on the reflecting loops (a) at 2.45 GHz. (b) at 5.25 GHz. (c) at 2.45 GHz in ON-state. (d) at 2.45 GHz in Off-state. (e) at 5.25 GHz in ON-state. (f) at 5.25 GHz in Off-state.	43
Fig. 4.12. (a) The simulated current distribution at 5.25 GHz when two transmission line connects. (b) The transmission coefficient curves when two transmission lines connect or disconnect.	44
Fig. 4.13. The geometry of the dual-band feeding antenna.	45
Fig. 4.14. The measured and simulated return loss of the dual-band feeding antenna.	46
Fig. 4.15. The photo of the realized dual-band pattern reconfigurable antenna.	47
Fig. 4.16. The measured return losses in Case 1 and Case 2.	49
Fig. 4.17. The measured and simulated radiation patterns in $\phi = 45^\circ$ -plane in Case 2 at (a) 2.55 GHz. (b) 5.25 GHz.	50
Fig. 4.18. The measured and simulated radiation patterns in xz- and yz-plane in Case 1 at (a) 2.55 GHz. (b) 5.25 GHz.	51
Fig. 5.1. The configuration of the proposed dual-band pattern reconfigurable antenna.	52
Fig. 5.2. The configuration of the simulated assignment.	54
Fig. 5.3. The geometry of the dual-band switching reflector.	54
Fig. 5.4. (a) The current distribution on the loop in on- and off-state at 2.45 GHz. (b) The radiation patterns in ON- and Off-state at 2.45 GHz.	55
Fig. 5.5. (a) The current distribution on the loop in on- and off-state at 5.25 GHz. (b) The radiation patterns in ON- and Off-state at 5.25 GHz.	56
Fig. 5.6. The effects of the increment of the width, W_{lp} . (a) The current distribution on the loop in ON- and Off-state at 5.25 GHz. (b) The radiation patterns in on- and off-state at 5.25 GHz.	57

Fig. 5.7. The effects of the increment of the width, L_{lp} . (a) The current distribution on the loop in on- and off-state at 5.25 GHz. (b) The radiation patterns in on- and off-state at 5.25 GHz. 58

Fig. 5.8. The geometry of the center dual-band feeding antenna. 59

Fig. 5.9. The measured and simulated results of the center dual-band feeding antenna. . 60

Fig. 5.10. The photo of the complete dual-band pattern reconfigurable antenna. 61

Fig. 5.11. The measured and simulated results of the return losses in Case 1..... 63

Fig. 5.12. The measured and simulated results of the return losses in Case 2..... 63

Fig. 5.13. The measured and simulated radiation patterns in $\phi=45^\circ$ -plane in Case 2 at (a) 2.55 GHz. (b) 5.25 GHz. 64

Fig. 5.14. The measured and simulated radiation patterns in xz- and yz-plane in Case 1 at (a) 2.55 GHz. (b) 5.25 GHz..... 65



Chapter 1 INTRODUCTION

In recent years, wireless communication has attracted lots of attentions. Numerous wireless devices are invented to bring convenience to people and a great many standards for wireless communication are defined continuously. Due to more and more requirements for communication devices, a communication device capable of using in multiple frequency bands becomes more and more common. The wireless communication standards, IEEE 802.11a/b/g/n, are one of the popular frequency bands to use for wireless internet connection. These standards are listed as the TABLE I.

TABLE I
THE IEEE STANDARDS OF 802.11 A/B/G/N

802.11 Protocol	Release	Freq. (GHz)	Typ. Throughput (Mbit/s)	Max net bitrate (Mbit/s)	Mod.	r_{in.} (m)	r_{out.}(m)
–	1997	2.4	0.9	2		~20	~100
a	1999	5	23	54	OFDM	~35	~120
b	1999	2.4	4.3	11	DSSS	~38	~140
g	2003	2.4	19	54	OFDM	~38	~140
n	2008	2.4, 5	74	248	OFDM	~70	~250

The operating frequency band in 802.11a is from 5.14 GHz to 5.875 GHz, while 802.11b, 802.11g and 802.11n standards operate in the 2.4 GHz band. Nevertheless, IEEE 802.11a/b/g/n is not licensed by departments of our governments or the international organizations. Many wireless devices, such as cellular phones, Bluetooth

devices and wireless internet cards, share these bands so interferences between each device are severe in these frequency bands. Moreover, multi-path problems caused by lots of barriers located within the environment for wireless communication are still challenging our technologies. Many solutions are actively proposed and continuously under development. One of the possible solutions is a smart antenna.

Smart antennas (also known as adaptive array antennas, multiple antennas and recently MIMO) refer to antenna arrays with smart signal processing algorithms used to identify spatial signal properties such as the direction of arrival (DOA) of the incoming signal, and use it to calculate beam-forming vectors, to track and locate the antenna beam on the mobile target [1]. Smart antenna techniques are operated especially in acoustic signal processing, track and scan RADAR system, radio astronomy and radio telescopes, and mostly in cellular systems like W-CDMA and UMTS. In addition, there are two major functions, estimation of the direction of the arrival signal and beam-forming technique, in designs of smart antennas.

The smart antenna system estimate the direction of the arrival signal through techniques such as Multiple Signal Classification (MUSIC), Estimation of Signal Parameters via Rotational Invariant Techniques (ESPRIT) algorithms, Matrix Pencil method or one of their derivatives. They are used to find a spatial spectrum of the antenna or sensor array, and calculate the DOA from the peaks of this spectrum. After finding out the DOA of the tracked device, then beam-forming technique is used to increase the system performance.

Beam-forming technique is the method used to create the radiation pattern of the antenna array by adding constructively the phases of the signals in the direction of the desired targets/mobiles, and canceling the pattern of the targets/mobiles that are undesired/interfering targets. The constructive phases can be changed adaptively to provide optimal beam-forming patterns with motions of the targets/mobiles, in the sense that it reduces the Minimum Mean Square Error (MMSE) between the desired and actual beam pattern formed. Beam-forming technique can be classified into two of the main categories: conventional switched beam antennas and adaptive array antennas. Conventional switched beam antennas have several available fixed beam patterns formed by the combinations of a fixed set of weightings and phasings from the sensors in the

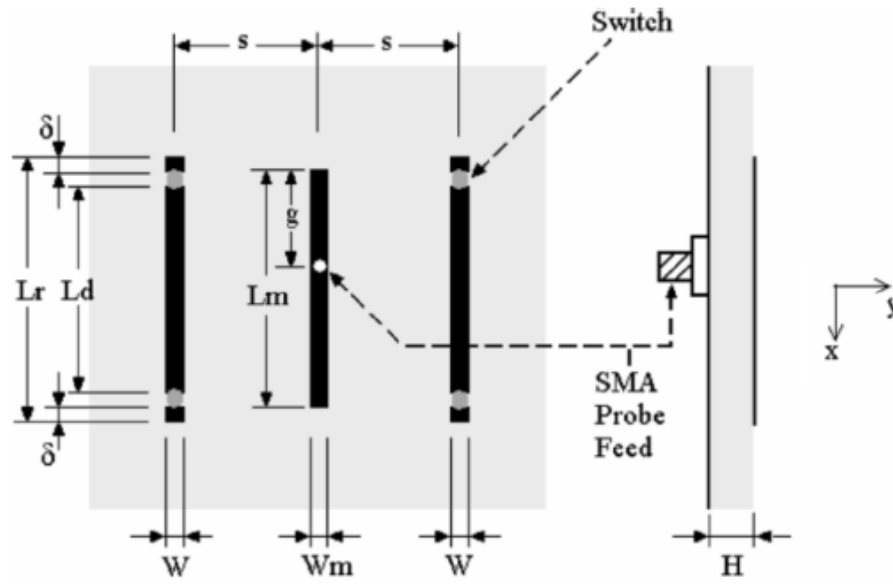


Fig. 1.1. Geometry of a 2-D pattern reconfigurable antenna based on Yagi-Uda antennas.

array. By periodically switching those fixed beam patterns, the whole area can be scanned, but the main beam of the antenna pattern cannot focus on the direction of the arrival signal to continuously enhance the receiving signal. In contrast, adaptive array antennas can switch its main beam to the direction of the arrival signal smartly by combining and analyzing the collecting information of the arrival signal. Then, they can fix their main beam at the desired signal until the desired signal moves or stops. Apparently, adaptive antenna systems are the better design consideration to solve the interference and multi-path problems in wireless communication environments.

For utilizing the limited spectrum efficiently, lots of pattern diversity antennas have been proposed [2]-[20]. They are good candidates to reduce the interference caused by multi-path situations and other devices and increase the power efficiency due to adaptive beam-forming patterns and high directional gain. Many of pattern reconfigurable antennas are developed from the Yagi-Uda antenna design [1]-[14]. In a Yagi-Uda antenna, if the length of the parasitic element is shorter than that of the active element, it will have a pulling pattern in the direction from the active element to the shorter parasitic element. Contrarily, if the length of the parasitic element is longer than that of the active element, it will have a pushing pattern in the direction from the longer parasitic element to the active element. Consequently, by arranging parasitic elements with different

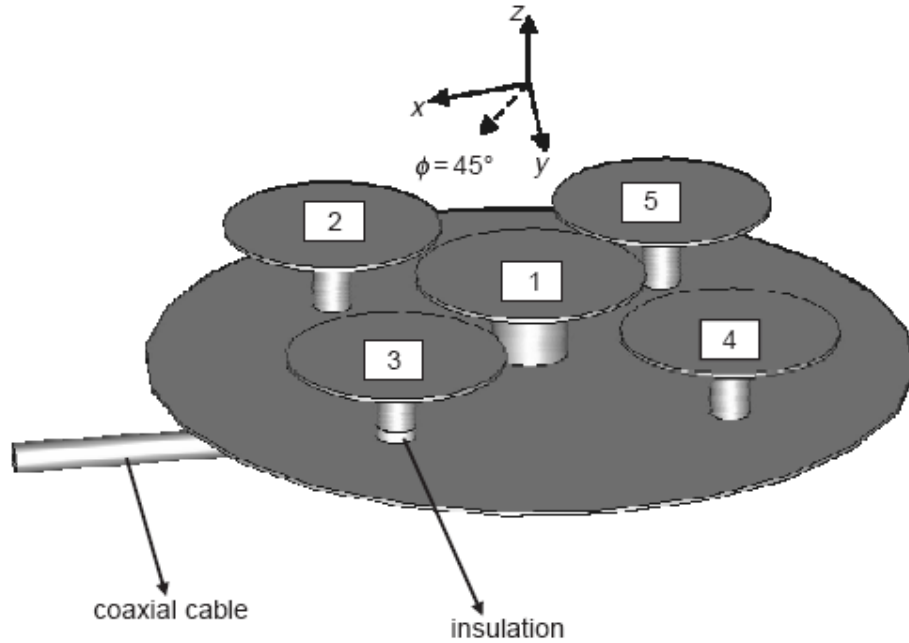


Fig. 1.2. Geometry of a 3-D pattern reconfigurable antenna based on Yagi-Uda antennas.

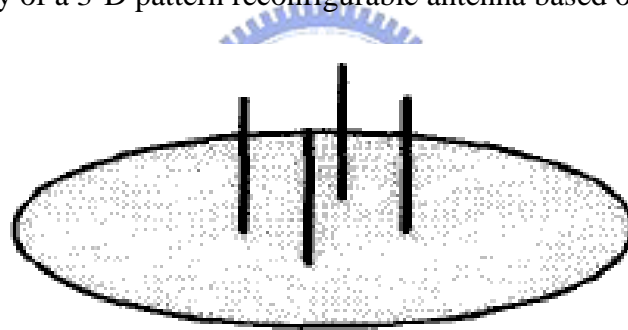


Fig. 1.3. Geometry of a 3-D pattern reconfigurable antenna by changing feeding locations

lengths around the active elements, various patterns can be achieved. Furthermore, switches can be loaded on each parasitic element to change the length of each parasitic element easily and electronically [12]-[13]. In [2]-[3], a feeding monopole antenna is positioned between two parasitic elements with two switches on each one, as shown in Fig. 1.1. By controlling the two switches on each element at the same time, an element which is longer or shorter than a feeding monopole is easily achieved. By the combinations of the length variations of parasitic elements, three different patterns can be accomplished. The above one is a 2-D structure, and a 3-D structure is introduced in [4]-[6]. As shown in Fig. 1.2, the parasitic elements can be switched to open-circuit to the ground plane to form a director. Increasing the number of parasitic elements in each

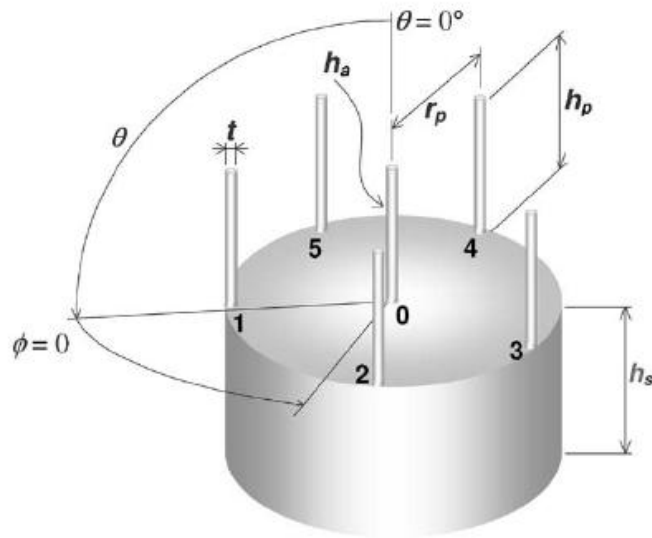


Fig. 1.4. Geometry of a 3-D pattern reconfigurable antenna with circle arrangement of parasitic elements.

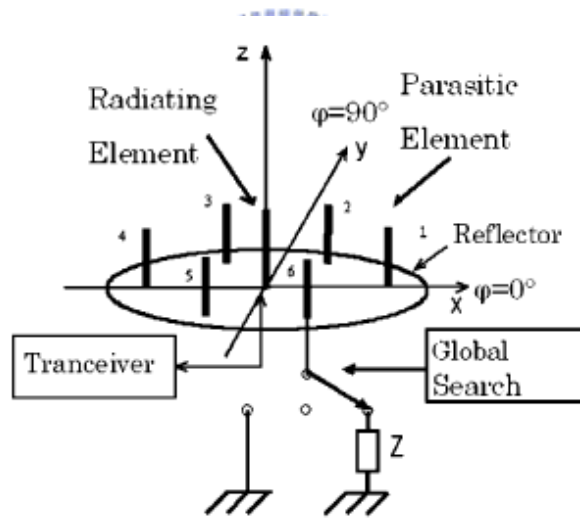


Fig. 1.5. A pattern diversity antenna by changing the induced current distribution on parasitic elements.

direction can enhance the directivity of the antennas, and stuffing substrate within the area where active and parasitic elements are located can reduce the total size of the proposed antenna [7].

Moreover, the cylinder rod monopole with disc plates can help reducing the height of the proposed antenna. In [8]-[9], changing the feeding antenna is a good way to switch patterns by using other antennas as parasitic elements, as shown in Fig. 1.3. Some

configurations of the parasitic elements are arranged in the shape of circle [10]-[12] to form more directional patterns, as shown in Fig. 1.4. In addition to changing length of parasitic elements, changing the induced current distribution on parasitic elements is also capable of switching patterns [12]-[14]. As shown in Fig. 1.5, using switches with three poles to change a parasitic element to be open-circuit, short-circuit or loaded causes variations of current distribution to switch patterns.

In the above mention to pattern diversity antennas, they operate only at single frequency band. Those single-band operations cannot be satisfied by users nowadays. In this thesis, we proposed three novel dual-band pattern diversity antennas. These antennas evolve from the right angle corner reflector antenna with combinations of the frequency selective surface (FSS) structures. Each frequency selective surface on the wall can be controlled by one switch. A dual-band feeding antenna is located at the center of the corner reflector antenna. The first proposed dual-band pattern diversity antenna consists of two-layer FSS walls that the four inner walls at four directions respectively are for higher frequency and the four outer walls at four directions respectively are for lower frequency. Eight switches are enough to obtain the pattern diversity. Basically, the patterns that we switch are the omni-directional pattern and the directional pattern caused by the corner reflectors. The second dual-band pattern diversity antenna is a progression from the first one. Only one-layer walls are needed to keep dual-band operation. Its size is much smaller than the first proposed antenna's size. There are two FSS structures printed on each wall, which are for higher frequency and for lower frequency, respectively. Besides, fewer switches are needed: only four switches are enough for using in dual bands. At the end, the third dual-band pattern diversity antenna is proposed. In the second antenna, two FSS structures are used to operate at dual bands, but only one FSS structures are needed in the third proposed antenna. Its structure is very simple to fabricate. The results of the third antenna are almost the same as the results of the second one. Similarly, only four switches are required here. All of the proposed antennas feature beam tilting property caused by the ground under the feeding antennas and reflecting walls. This property can reduce the co-channel interference. Therefore, they are greatly suitable for modern base station antenna applications.

Chapter 2 THEORY OF THEORY OF CORNER REFLECTOR ANTENNA AND FREQUENCY SELECTIVE SURFACE

2-1 CORNER REFLECTOR ANTENNA

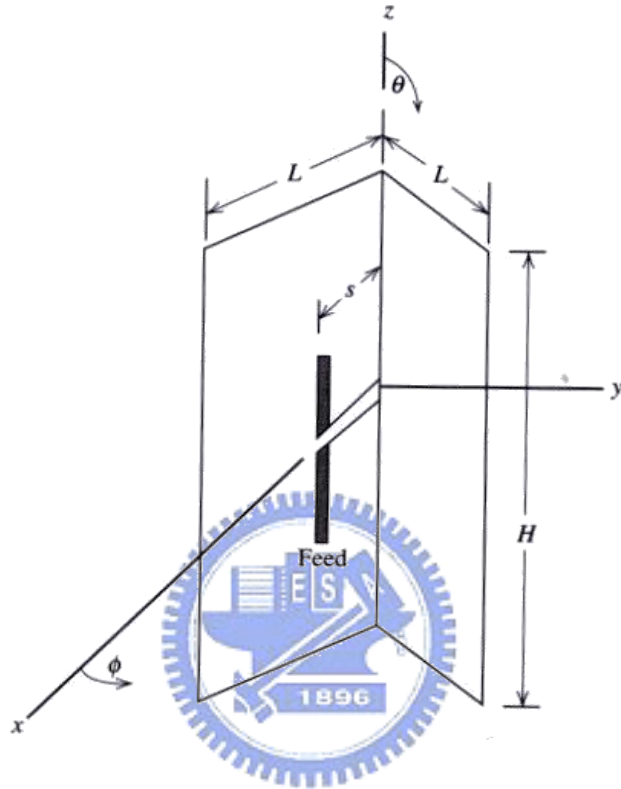


Fig. 2.1. The configuration of a corner reflector antenna.

Based on the content in [15], corner reflector antennas are a good candidate to obtain a good gain and directivity in our antenna design. As shown in Fig. 2.1, a half-wavelength dipole is in the area with two metal plates which form a corner with particular angle. A corner reflector antenna with 90° angle is the most practical one. The corner reflector antenna can be analyzed by the image theory and the array principle, as shown in Fig. 2.2. After analyzing, we can find that the pattern shape, gain, and feed point impedance will all be a function of the spacing between the feed point and the corner, s . A good directivity can be achieved if $0.25\lambda \leq s \leq 0.7\lambda$ when the metal plates are of infinite extent, but the input impedance of a dipole feed will be around 125Ω which does not match to the usual port impedance, 50Ω . As shown in Fig. 2.3, the best spacing, s , is 0.5λ .

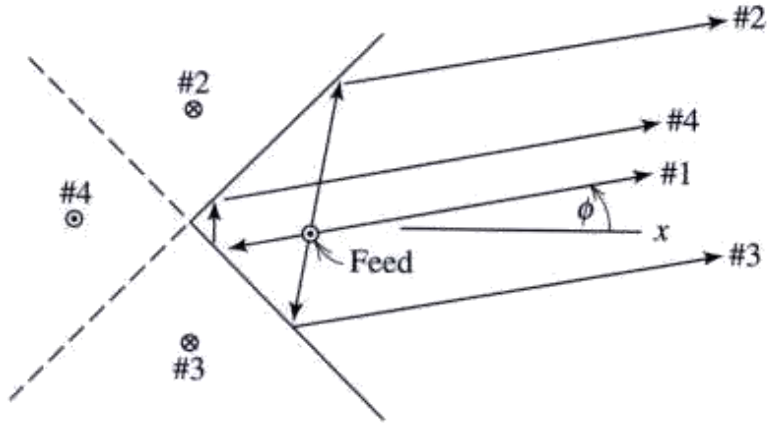


Fig. 2.2. The corner reflector with images shown and how they account for reflections.

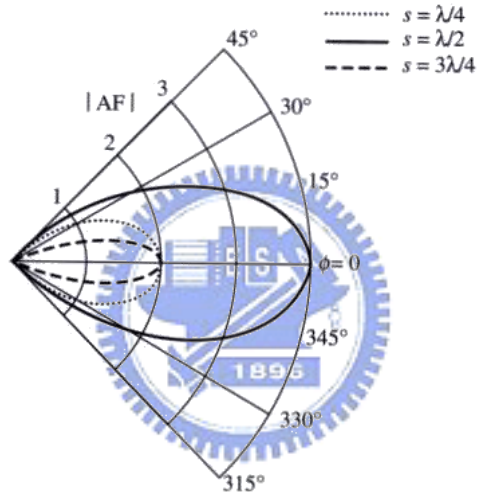


Fig. 2.3. Principal plane patterns, $|AF|$, for a right angle corner reflector.

Therefore, we have to find a balance condition between good directivity and well-matching input impedance.

In real world, infinite metal plates are impossible to fabricate. Therefore, making the metal plates finite is necessary. By ray tracing, that the length of the metal plate of $L=2s$ is an acceptable dimension in corner reflector antenna design to keep the directivity but with a broader main beam. The height of the metal plate, H , is suitable to use from 1.2 to 1.5 times the length of the feed element to minimize the direct radiation by the feed into the back region of the metal plates.

There are some corner reflector antennas proposed [16]-[20]. In Fig. 2.4, a three dimensional corner reflector antenna is introduced [16]. With the conducting plane under

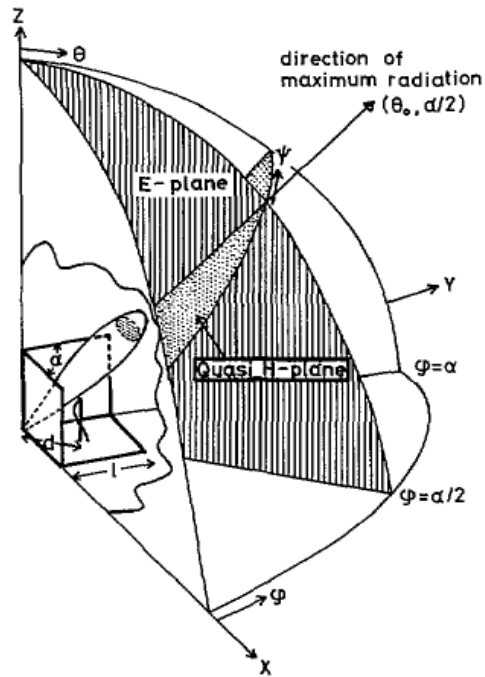


Fig. 2.4. Geometry of a three-dimensional corner reflector antenna.

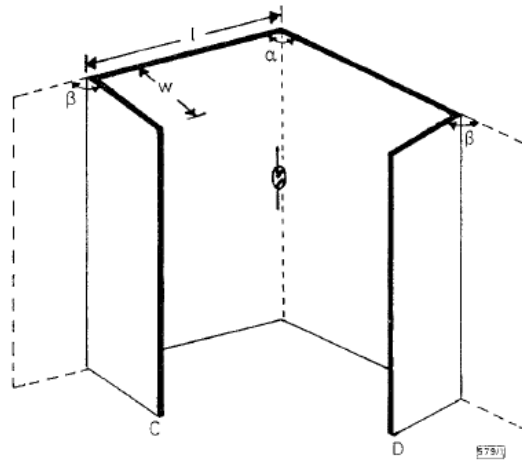


Fig. 2.5. Geometry of a triple corner reflector antenna.

the feeding element, the main beam will tilt and become narrower. In [18], a triple corner reflector antenna can narrow the main beam by two more corners, as shown in Fig. 2.5. Besides, using a cylindrical corner in the corner reflector antenna can increase the maximum gain because more image sources with constructive interference can be produced in Fig. 2.6[19]. Finally, a switching corner reflector antenna has been proposed [20]. As shown in Fig. 2.7, by controlling the lengths of the parasitic elements on the

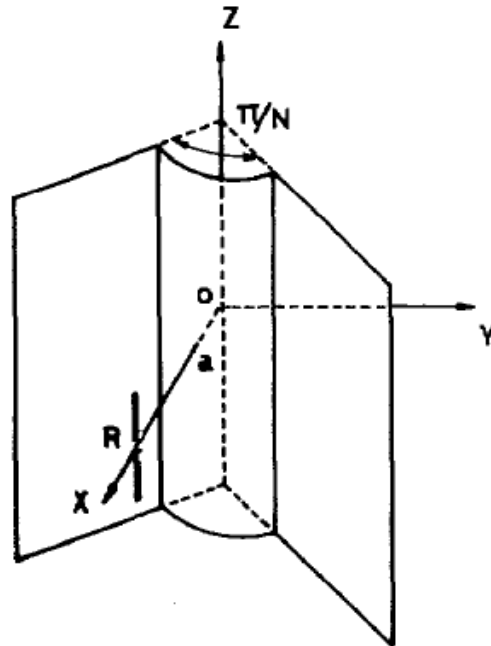


Fig. 2.6. Geometry of a corner reflector antenna with the cylindrical corner.

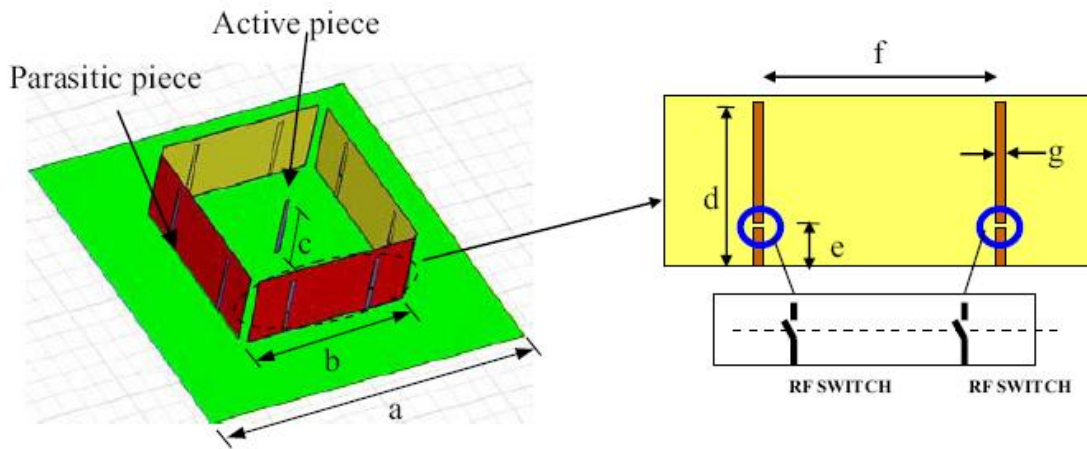


Fig. 2.7. Geometry of a pattern reconfigurable antenna evolved from Yagi-Uda antennas and corner reflector antennas.

reflecting walls to reflect or to pull the antenna patterns, this corner reflector antenna can switch its main beam in four directions. These ideas are similar to the antenna designs we proposed in this thesis.

2-2 FREQUENCY SELECTIVE SURFACE

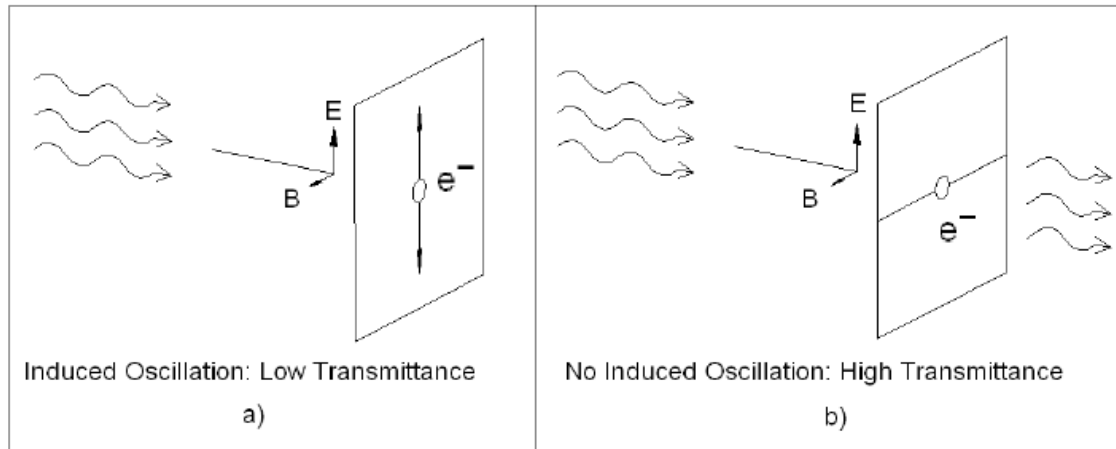


Fig. 2.8. (a) An electron in filter plane undergoes oscillations driven by source wave. (b) An electron constrained to move along wire cannot undergo oscillations.

Frequency selective surface (FSS) is any surface construction designed as a ‘filter’ for plane waves. It evolves from Radar Cross Section (RCS) with angular/frequency dependence. It has band pass/band stop behavior just like a conventional filter. Basically, it is a periodic structure in 2-D, typically, with narrow frequency bandwidth [21]. The operating principle of the FSS can be found in [22]. As shown in Fig. 2.8(a), a vertically polarized plane wave incident from the left side which strikes a metal plane at normal incidence. We can imagine what happens to a single electron located in the metal plane when the wave strikes the filter. Because the plane is orthogonal to the moving direction of the incident waves, the electronic field of the source lies in the plane. This electronic field exerts a force on the electron and causes it to oscillate if the condition is appropriate for oscillation. A portion of the energy from the incident waves must be converted into kinetic energy in order for the electron to remain in the oscillating state. To preserve conservation of energy, only a fraction of the incident power will be transmitted and the rest is absorbed by the electron. Then, the absorbed energy will be re-radiated from the oscillating electron. This re-radiated field cancels the electronic field at the backside of the FSS structure, and the FSS structure reflects the field back. If all of the energy from the wave is transferred to electrons in the metal or the backside fields are cancelled, then the transmittance through the filter will be zero. Next, now imagine a different situation.

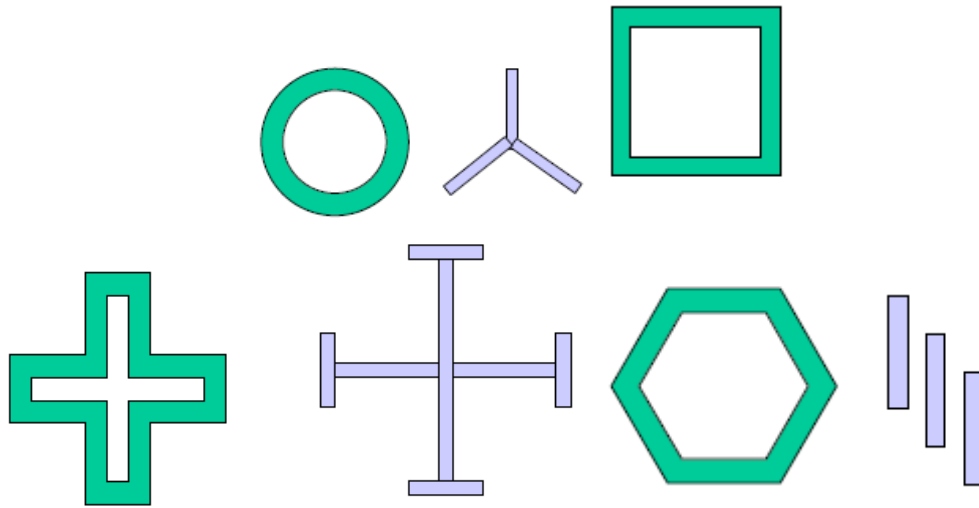


Fig. 2.9. Different shapes of the FSS structures.

Think about that we have a line which lies in the metal plane but it also orthogonal to the E-field of the incident plane wave, as shown in Fig. 2.8(b). If an electron is limited to move along this wire, it will not be able to absorb kinetic energy from the incident wave because it is not allowed to accelerate in the direction that the force is exerted. In this case, the electron is effectively invisible to the incoming wave which will be fully transmitted.

Based on the theory of the FSS structure, numerous FSS structures are proposed in Fig. 2.9 [21]. Based on the shapes, sizes, loads and spacing between each element, we can determine the operating frequencies. Then, according to the orientation of each element, the dependence on polarization can be decided. Besides, recently, some dual-band FSS structures are proposed by implemented multiple resonant circuits [23]-[24].

Chapter 3 DUAL-BAND PATTERN RECONFIGURABLE ANTENNA WITH TWO-LAYER WALLS

3-1 ANTENNA CONFIGURATION

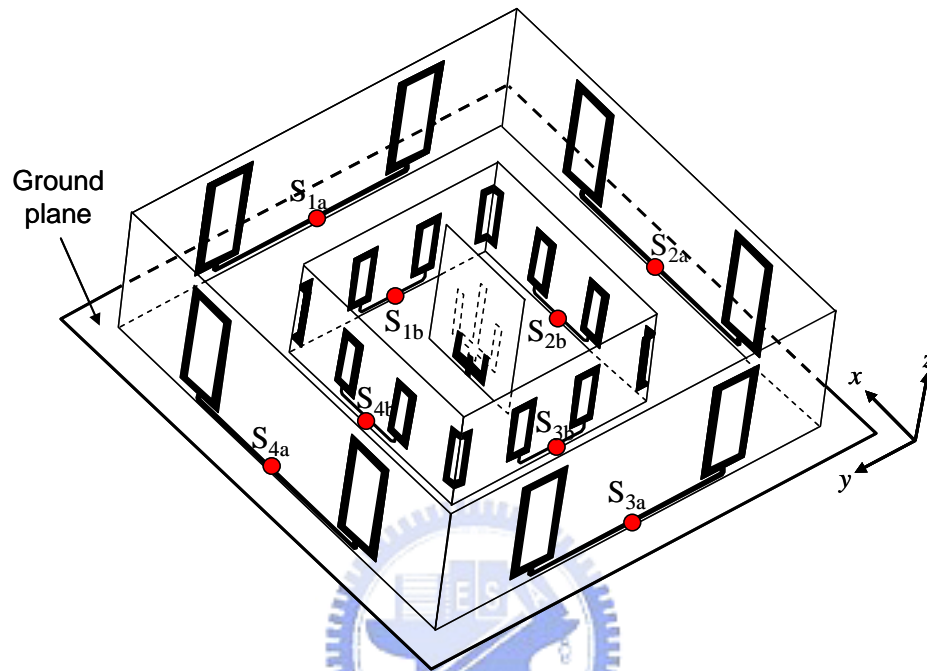


Fig. 3.1. Configuration of the proposed dual-band pattern reconfigurable antenna.

Based on theories of the corner reflector antenna and the frequency selective surface, we combined them together to form a new dual-band pattern reconfigurable antenna. As shown in Fig. 3.1, a dual-band pattern reconfigurable antenna comprises a center dual-band feeding antenna, four small-size rectangular plates at the inner sidewalls, four large-size rectangular plates at the outer sidewalls and a finite ground plane. The inner and outer sidewalls consist of switching FSS structures printed on the FR4 substrate with thickness of 0.8 mm. The inner walls can control patterns at higher frequencies, 5.25 GHz, while the outer walls can control patterns at lower frequencies, 2.45 GHz. Their properties of transmission and reflection are controlled by the switch states at the center of each wall. The switches are located between the center point of a metal control line and a ground. At one of the switch states, the FSS wall acts as a reflector which can block the electromagnetic waves at operating frequencies whereas at the other switch state, it becomes transparent to the electromagnetic waves at operating frequencies. When a

switch is passable, the center point of a metal control line and a ground plate are connected while when it is impassible, they are separated. In Fig. 3.1, $S_{1a}\sim S_{4a}$ and $S_{1b}\sim S_{4b}$ are names of the switches located at the outer walls and the inner walls, respectively. According to the combinations of the switches at the inner and outer sidewalls, various patterns can be achieved at two frequency bands.

Based on the theory of the corner reflector antenna, the spacing between a reflecting wall and a feeding antenna is 0.5 wavelength. Therefore, the size of the ground plate is determined by the lower operating frequency, 2.45 GHz. The ground plate is fabricated on the FR4 substrate, whose thickness is 0.8 mm and whose dielectric constant is 4.4, with dimension of 140 mm \times 140 mm.

The driving element, which is a dual-band antenna, is located at the center of the ground plate. It is designed for 2.45 GHz and 5.25 GHz. This antenna, which is perpendicular to the ground plate, is printed on the both side of the FR4 substrate with dimension of 40 mm \times 30 mm \times 0.8 mm. In addition, the matching microstrip line for the feeding antenna is made on the other of the substrate of the ground.

Besides, the associated circuitry of the switch, such as bias lines and RF chokes, can be fabricated on the backside of the ground plate to prevent the on-going electromagnetic waves from the unwanted influence by them because they are not showing in the path of electromagnetic waves.

According to the corner reflector antenna, the best spacing to get the best forward gain between the reflector wall and the feeding element is 0.5 wavelength therefore the spacing of the inner sidewall and the feeding antenna is 30 mm and that of the outer sidewall and the feeding antenna is 60 mm.

In the following section, we will discuss about the design of them.

3-2 DESIGN OF RECONFIGURABLE FSS STRUCTURES

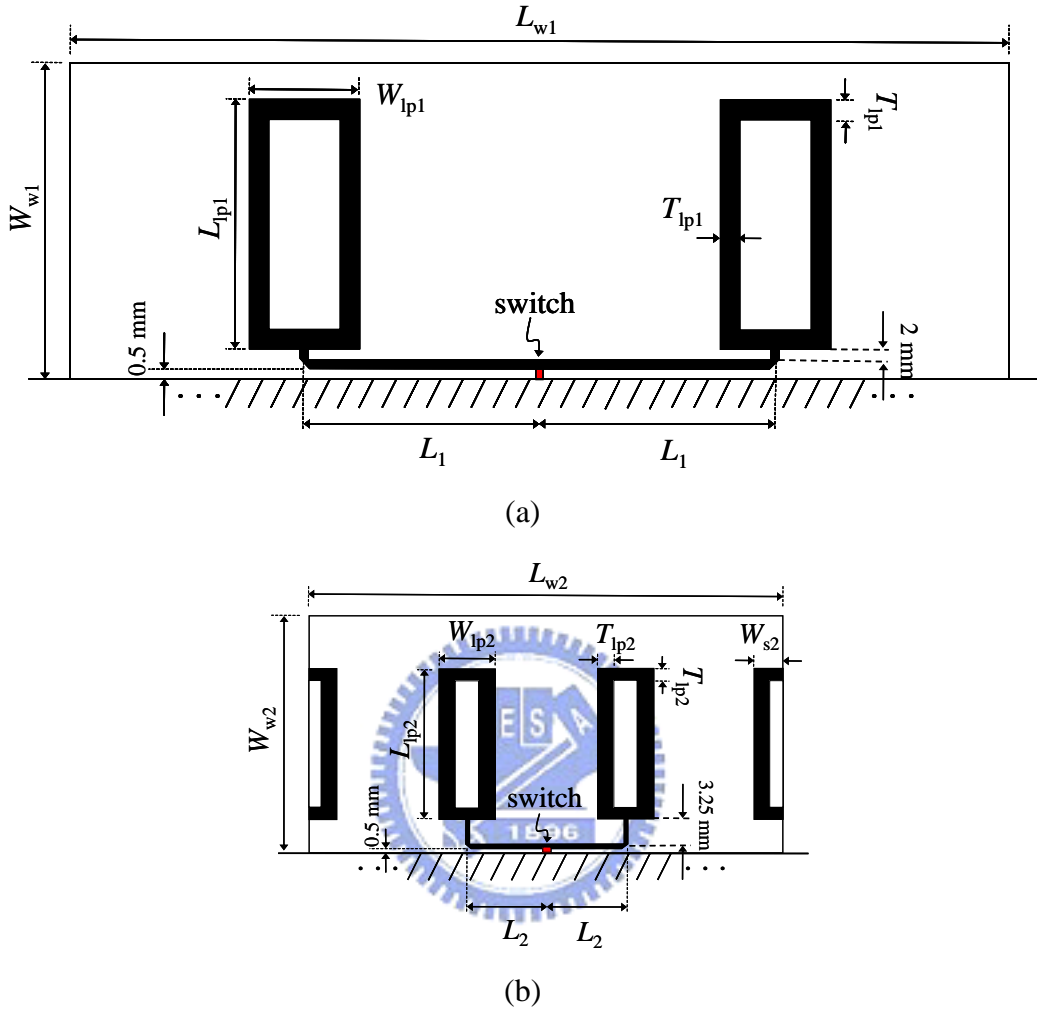


Fig. 3.2. Geometries of the dual-band FSS structures (a) the outer walls (b) the inner walls

In our proposed antenna, we focus on the vertical polarization. Referring to Chapter 2.2, among lots of FSS structures, we choose a rectangular loop to be our design of the FSS structure because it is easier to design the FSS for particular polarization. Therefore, we have to make the vertical arms of the rectangular loops longer than the horizontal arms of it to make this FSS structure only respond to vertical polarization.

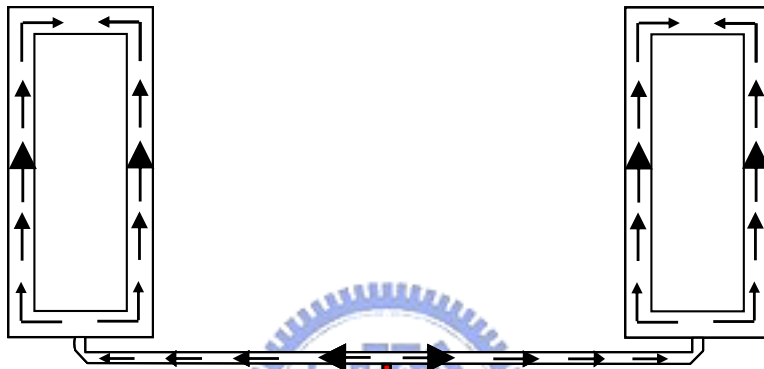
The geometries of the dual-band FSS structures are shown in Fig. 3.2. These walls are perpendicular to the ground plate. They consist of two rectangular loops and a metal control line connecting two rectangular loops together. In Fig. 3.2(a), the FSS structure with $(L_{w1}, W_{w1}) = (120 \text{ mm}, 40 \text{ mm})$ is designed for operating at 2.45 GHz. Two parallel

rectangular loops are built to form the FSS structures. The circumference of a rectangular loop to be a FSS is one wavelength. L_{lp1} and W_{lp1} are the length and the width of the rectangular loop, and they are 32 mm and 14 mm, respectively. The thickness of the rectangular loop, T_{lp1} , is 2.5 mm. The distance between the two parallel rectangular loops is about half wavelength of the operating frequency. Therefore, the length of the printed metal control line connecting two rectangular loops is about half wavelength too. L_1 is the horizontal distance between the center point of the metal line and the center point of the rectangular loop with length of 30 mm. The gap between the metal line and the ground plate is 0.5 mm, and it is a location for mounting a switch. In Fig. 3.2(b), the definitions of the parameters of the FSS structures for 5.25 GHz are the same as that for 2.45 GHz except for W_{side2} . Its parameters, $(L_{w2}, W_{w2}, L_{lp2}, W_{lp2}, T_{lp2}, L_2)$, are (60 mm, 30 mm, 19 mm, 7 mm, 2 mm, 10 mm). As shown in Fig. 3.2(b), we can see that the configuration of the inner sidewalls is different from that of the outer sidewalls. We add two half rectangular loops at each side of the wall with the same length as the center rectangular loops and with $W_{s2} = 3.5$ mm. They can form extra loops with other two nearby inner walls in the configuration of the proposed antenna to increase the directivity of the patterns at 5.25 GHz. We will discuss its function later.

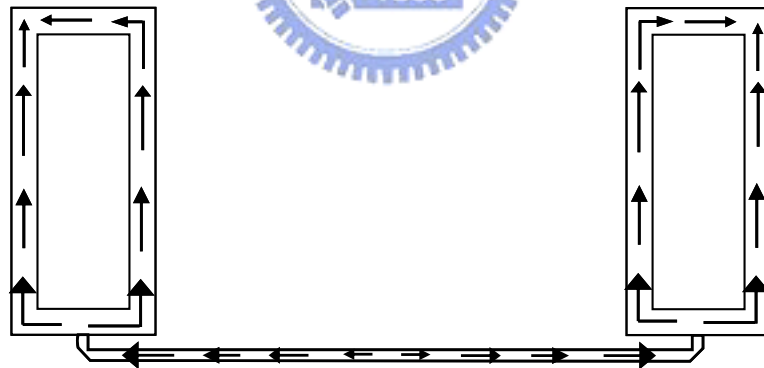
The FSS structures are controlled by the switch states and the metal transmission line. First, we define that when a switch is passable, which means that the center point of the metal transmission line and the ground plane are connected, we call this switch state “on”; otherwise, we call it “off”. Now we start to discuss about the working mechanism of the switching FSS structures. At the beginning, we can see the current distribution at 2.45 GHz when the FSS structures without the control transmission line. When the FSS structure is hit by vertically polarized electromagnetic waves, it will resonate at the operating frequency when its circumference is about one wavelength of the operating frequency which is 2.45 GHz in this case. Due to resonance, they will be excited strong current distribution which has strong current at the center of the vertical arms and current null at the center of the horizontal arms, as shown in Fig. 3.3(a). Then, these current re-radiate electromagnetic waves, which cancel the on-going electromagnetic fields at the backside of the wall and enhance the fields in front of the walls if the spacing between



(a)



(b)



(c)

Fig. 3.3. Current distributions of the FSS structures at 2.45 GHz on (a) two rectangular loops. (b) a switching FSS when the switch is on. (c) a switching FSS when the switch is off.

the feeding antenna and the reflector plate is adequate. As a result, it can reflect the on-going waves.

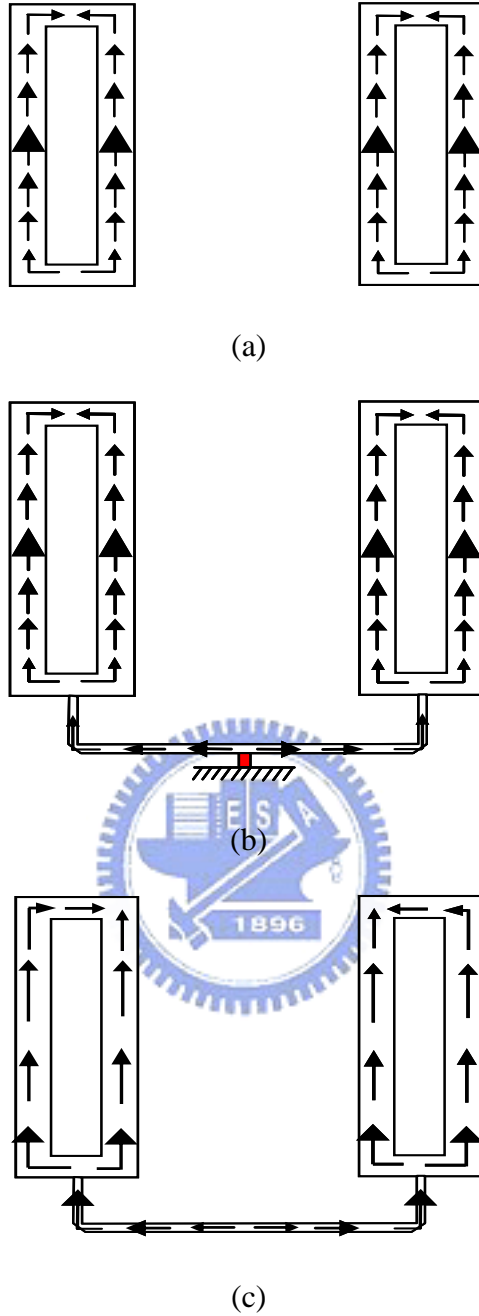


Fig. 3.4. Current distributions of the FSS structures at 5.25 GHz on (a) two rectangular loops. (b) a switchable FSS when the switch is on. (c) a switchable FSS when the switch is off.

Next, we consider a switching FSS with a metal control line. When the switch is “on”, the center point of the control line is short-circuit. Through the quarter-wave control line from the center point to the end point, open-circuit shows at the end point according to the transmission line theory [25]. As shown in Fig. 3.3(b), the resonant current

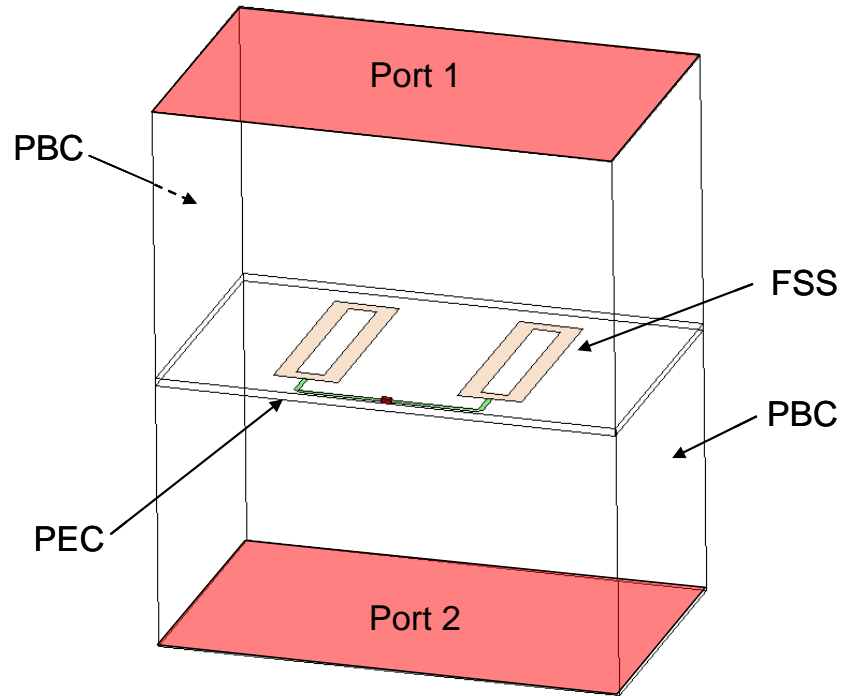
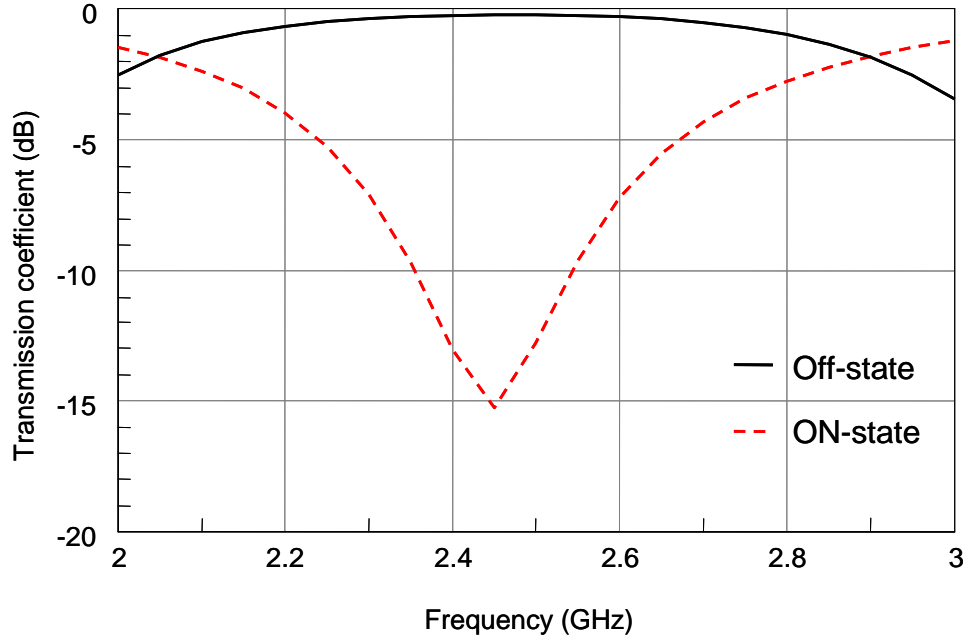


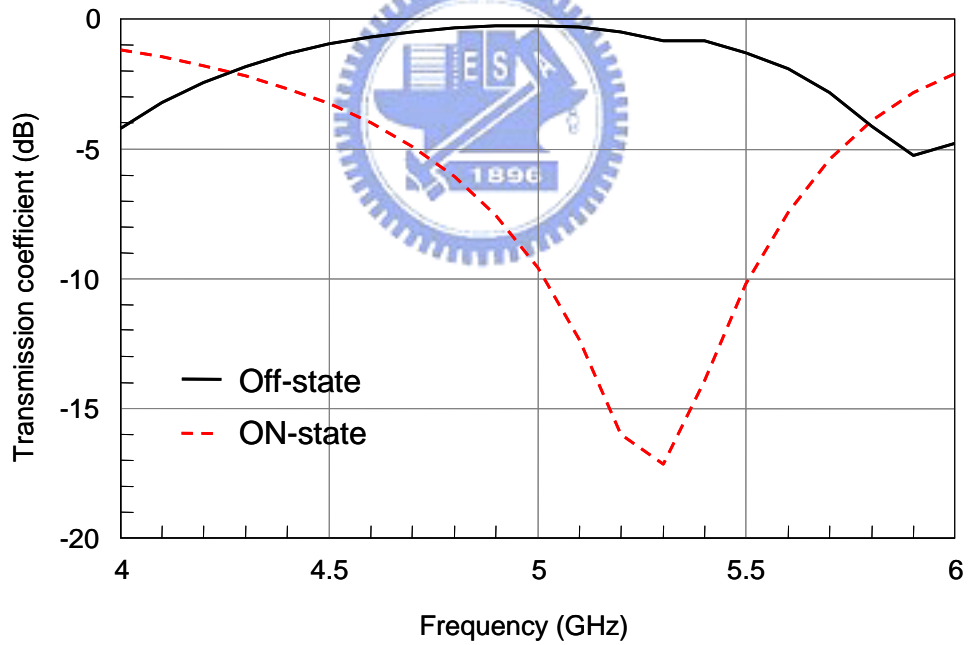
Fig. 3.5. The simulation model for designing FSS structures.

distribution on the rectangular loops will be kept the same as Fig. 3.3(a). As a result, this switching FSS structure reflects the incident waves just like the FSS structure made up of rectangular loops.

On the other hand, when the switch is “off”, the center point of the control line is separate from the ground plate. Based on the theory of symmetry, current null, which is similar to open-circuit, appears at the center point of the control line. Due to the quarter-wavelength control line, short-circuit shows up at both ends of the control line. Therefore, the resonant current distribution on the rectangular loops is destroyed. In Fig. 3.3(c), we can see that the current level is weaker than that of the above condition, even though the current distribution looks similar. Because of the weaker current level, the re-radiated electromagnetic fields by those current are too small to reflecting incoming waves. As a result, this FSS structure looks transparent to incoming waves. Incoming waves can pass through the walls easily. Based on above discussion, a switching FSS at 2.45 GHz is completed. The discussion of a switching FSS at 5.25 GHz is the same as that at 2.45 GHz. Its current distribution at 5.25 GHz is shown in Fig. 3.4.



(a)



(b)

Fig. 3.6. The simulated transmission coefficients at (a) 2.45 GHz (b) 5.25 GHz when the switches are in ON-state or Off-state.

The simulation method is shown in Fig. 3.5. The periodic boundary condition (PBC) is set at left and right sides of the wall to simulate the periodic condition of FSS. A

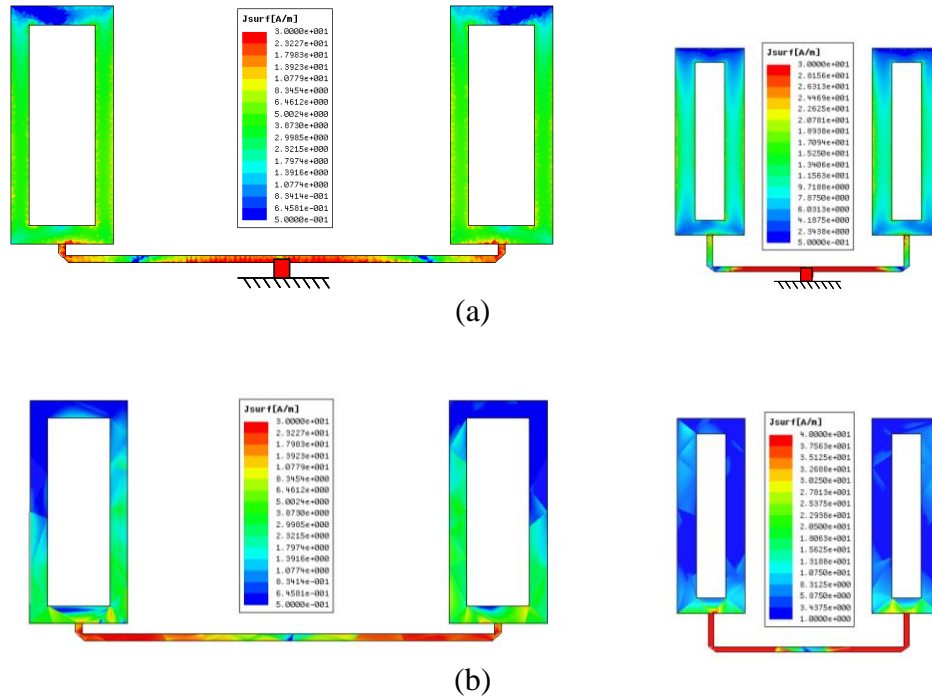


Fig. 3.7. The simulated current distributions in the dual-band pattern reconfigurable reflector antenna at 2.45 GHz (large loops) and 5.25 GHz (small loops) in (a) ON-state. (b) Off-state.

perfect conductor (PEC) is assigned to the plane under the wall. Then, two ports with vertical polarization are set at the upper and bottom plane to excite vertically polarized electromagnetic waves which are incident to FSS structures. The distance between one of the ports and the FSS structures is longer than quarter wavelength to make sure that the boundary condition at ports does not affect the proposed FSS structures in our simulations. In the beginning, we define that ‘ON-state’ is that the FSS walls can reflect the vertically polarized incident waves while ‘Off-state’ is that the FSS walls are transparent to the vertically polarized incident waves. The simulated transmission coefficients (S_{21}) are shown as Fig. 3.6. We can see that as the switches for 2.45 GHz and 5.25 GHz are on, the transmission coefficients at both frequencies are lower than -10 dB, which are -15.27 dB and -16.58 dB, respectively. They are good enough to prevent incoming waves from passing through the walls. On the other hand, when the switches are off, the transmission coefficients are higher than -1 dB, which are -0.208 dB and -0.684 dB, respectively. That means that all of incoming waves pass through the walls. The simulated current density distributions in ON-state and Off-state at both frequencies,

2.45 GHz and 5.25 GHz, are shown in Fig. 3.7. Vertically polarized incident waves are used to be a source. The results are similar to what we mentioned above. Due to the coupling effects between the rectangular loops and the transmission line, the open-circuit conditions do not really occur at the connecting points, as shown in Fig. 3.7(a). However, the resonances still remain on both structures. On the other hand, in Fig. 3.7(b), the current distribution on the rectangular loops in Off-state is weaker than that in ON-state.

After we completed our design of the switching FSS walls, a dual-band pattern reconfigurable reflector antenna can be fabricated by those walls operating at 2.45 GHz and 5.25 GHz.



3-3 DESIGN OF THE DUAL-BAND PATTERN RECONFIGURABLE REFLECTOR ANTENNA WITH TWO-LAYER WALLS

In this section, we will talk about the functions of the two more half rectangular loops on the inner wall, the interactions between the inner walls and the feeding antenna, and design of the feeding antenna. Here, we define that “Case 1” represents that all of the inner and outer switches are in off-state, which means that all of the walls are transparent to vertically polarized electromagnetic waves, and that “Case 2” represents that the switches, S_{1a} , S_{4a} on the outer walls and S_{1b} , S_{4b} on the inner walls, are in on-state, which means that a corner reflector antenna is formed and its directivity points to $\phi = 225^\circ$ at 2.45 GHz and 5.25 GHz.

3-3-1 Functions of the two more half rectangular loops printed on the inner wall

At the very beginning, there are only the center two rectangular loops and a metal control line printed on the FR4 substrate of the inner walls. Its parameters, $(L_{lp2}, W_{lp2}, T_{lp2}, L_2)$, are (10.5 mm, 6 mm, 2 mm, 15.25 mm). When we use it to be the inner FSS wall to reflect electromagnetic waves at 5.25 GHz, the simulated pattern of Case 2 is shown in Fig. 3.7. The dash line here represents the above simulated pattern. The directivity and the front-to-back ratio are not good enough for usage. The back lobe we define here is the direction at the angle between the maximum of the main lobe and the z axis at the other side of the z axis. To solve this problem, we add four corner loops to our proposed antenna configuration by implementing two half rectangular loops at both side of each inner wall. Due to increment of those corner loops, we have to reassign the positions of the center rectangular loops to form a periodic structure with a new period. When the switch is in on-state, the center rectangular loops and the corner loops form a good FSS structure to reflect waves at 5.25 GHz, and in Case 2, the corner rings can help to reflect the leak waves at the corner to increase the front-to-back ratio, as shown in Fig. 3.8. The solid line represents the simulated pattern of the modified antenna configuration, and it shows that the back lobe is much smaller than the previous one so its front-to-back ratio has been improved. On the other hand, when the switch is in off-state, the period formed by the corner loops is not adequate for FSS structures operating at 5.25 GHz. The

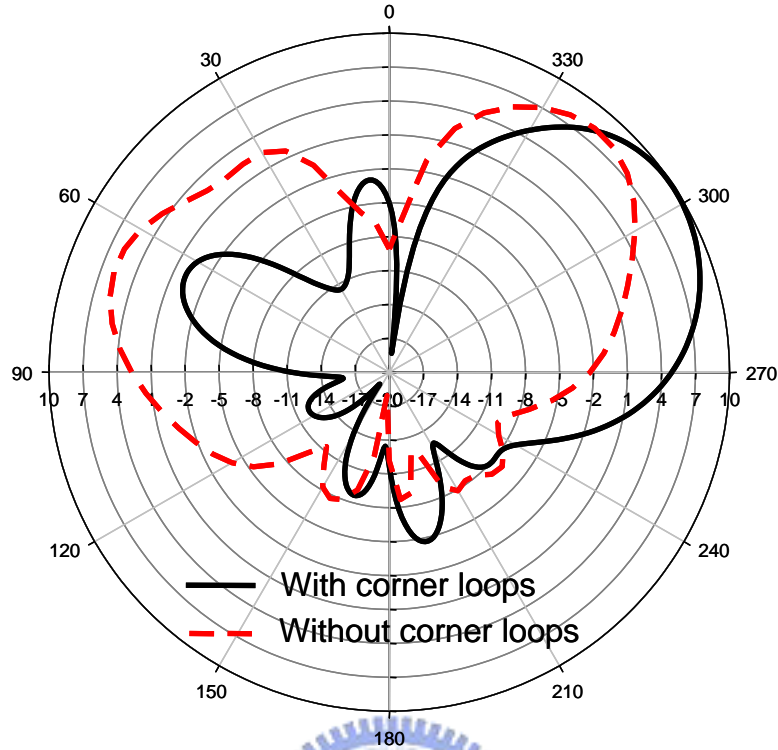


Fig. 3.8. The comparison of the patterns in $\phi = 45^\circ$ plane in case 2 at 5.25 GHz between the FSS wall for 5.25 GHz with corner rings and without corner loops.

walls look transparent to the incident waves just like the wall without corner loops. Consequently, the new proposed antenna can work well as a pattern reconfigurable antenna.

3-3-2 Interactions between the inner walls and the feeding antenna

In Fig. 3.9, the solid line shows the pattern at 2.45 GHz when only the outer walls work as a corner reflector while the dash line represents the pattern at 5.25 GHz when both inner and outer walls work as corner reflectors. We can see that the maximum gain of the solid line is smaller than that of the dash line. Based on the theory of Yagi-Uda antennas [15], a parasitic element which is shorter than a feeding element and is located in front of a feeding element act as a director to pull its radiation patterns out. Therefore, when the switch on the inner wall is in off-state, each side of the center rectangular loops with half of the control line forms a director at 2.45 GHz. As a result, the radiation pattern at 2.45 GHz is pulled out to spread at four directions to reduce the maximum gain of the main beam. Nevertheless, if the switch on the inner wall is in on-state, this current

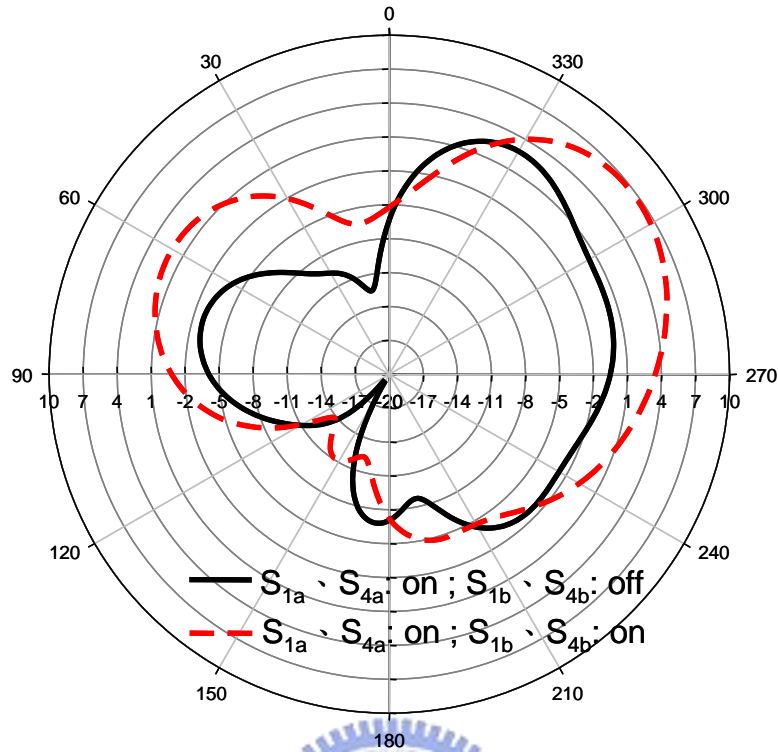


Fig. 3.9. The comparison of the patterns in $\phi = 45^\circ$ plane in case 2 at 2.45 GHz between the switches, S_{1b} , S_{4b} , in off-state and on-state.

distribution of the director is destroyed by connecting ground so it does not affect the pattern at 2.45 GHz. In conclusion, when we use this dual-band pattern reconfigurable reflector antenna, we have to make the switches in the same direction be in the same state, regardless of mounting on the inner or outer walls. Besides, we can just use one switch to control the inner and outer walls in the same direction at the same time to reduce the number of the switches for decreasing the cost.

3-3-3 Design of the feeding antenna

In this antenna design, we have to find an antenna which can have a good match in both cases. It is hard to design this kind of antenna because the electromagnetic field excited by an antenna in different cases is quite different from each other. Therefore, antenna design becomes one of the important designs in the proposed antenna module.

A proposed antenna is shown in Fig. 3.10. It consists of two trident structures that that the front and lower one is for 5.25 GHz and the combination of both trident structures is for 2.45 GHz. The parameters for the front trident structure, (H_1, B_1, A_1, D_1) , are (2 mm, 3

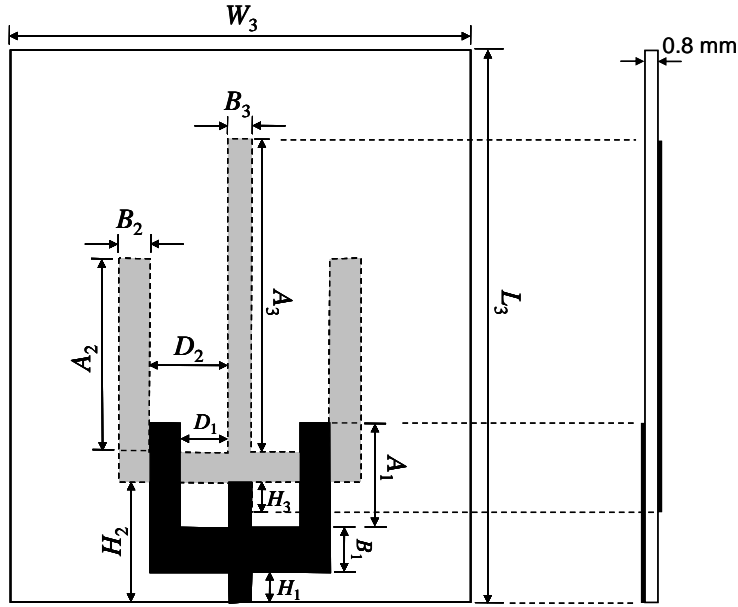


Fig. 3.10. The dual-band feeding antenna with two trident structures.

mm, 7 mm, 3.25 mm), and the parameters for the back trident structure, (H_2 , A_2 , B_2 , D_2 , A_3 , B_3 , H_3), are 8 mm, 13 mm, 2mm, 5.25 mm, 21mm, 1.5 mm and 2 mm, respectively. By tuning the values of A_1 and H_3 can change the amount of the coupling. To excite the higher frequency, we feed into the front trident structure directly by a microstrip line printed on the other side of the ground substrate. Its center arm is about quarter wavelength of 5.25 GHz. For the excitement of the lower frequency, we use the coupling effect between two trident structures. The total length of the center arm in the lower trident structure and the center arm in the higher trident structure is about quarter wavelength of 2.45 GHz. Besides, the arms at both sides can increase amounts of the coupling and increase the impedance bandwidth, especially at higher frequency band. The simulated and measured results are shown in Fig. 3.11. We can see that the impedance bandwidth which is lower than -10 dB at higher frequency band is from 3.12 GHz to 5.75 GHz and that at lower frequency is from 2.23 GHz to 2.64 GHz. The measured result is quiet similar to the simulated result at lower frequency band. The problems caused by fabrication may make the differences at higher frequency band. Basically, the range which is lower than -10 dB is almost the same as the simulated result at higher frequency band.

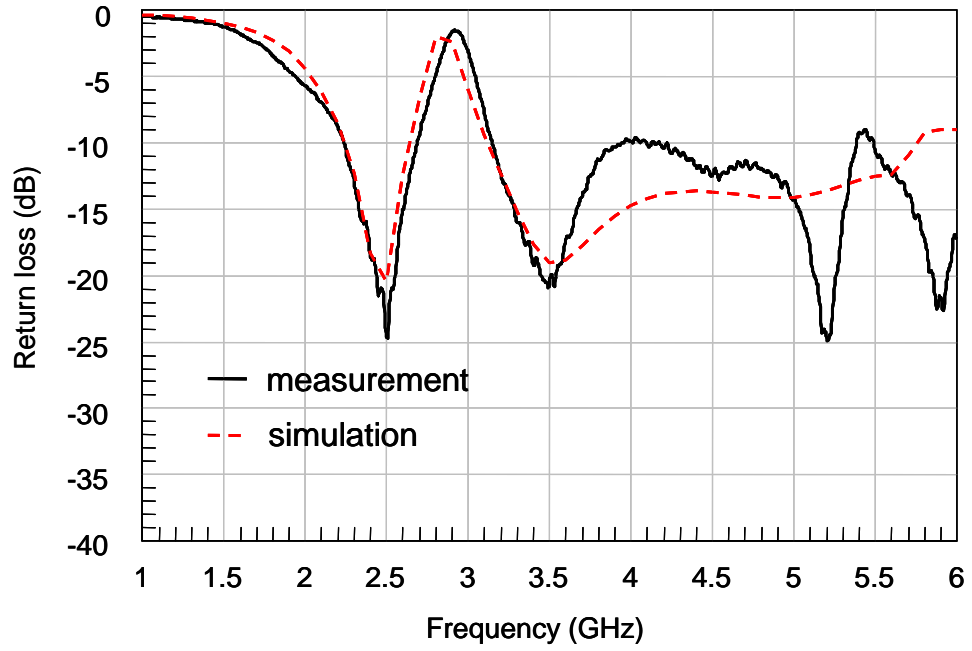


Fig. 3.11. The measured and simulated return loss of the dual-band feeding antenna.



3-4 MEASUREMENT RESULTS

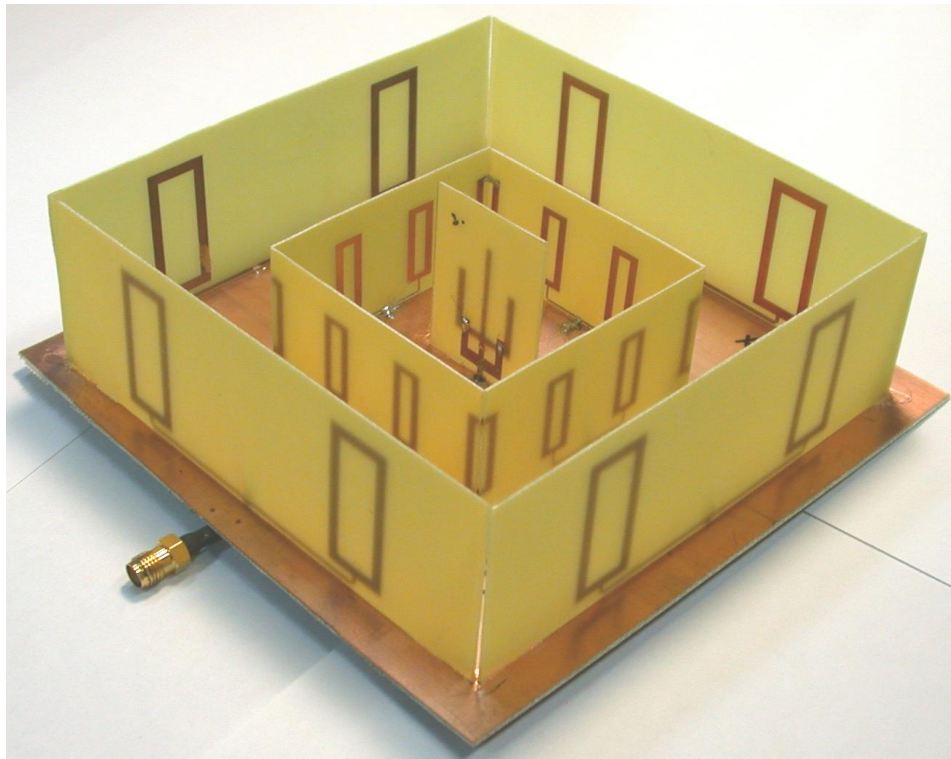


Fig. 3.12. The photo of the complete dual-band pattern reconfigurable reflector antenna.

The photograph of the complete dual-band pattern diversity antenna is shown in Fig. 3.12. Various patterns can be obtained by the combinations of the switch states. In real applications, the omni-directional and directional patterns are more important than others. We use the directional patterns to detect where the signal comes from and then focus on the direction of the signal to increase the receiving power of the signal and reduce the noise and the multi-path effects. Besides, we can use the omni-directional pattern to transmit the signals to each devices to save the transmission time. Consequently, we only focus on the results of the cases with the omni-directional and directional pattern, respectively. The definitions of both cases and the measured and simulated results at both cases are listed in TABLE II

The measurement results of return loss of case 1 (omni-direction) and the case 2 (direction) are shown in Fig. 11. In Case 1, it can be seen that the -10 dB bandwidth is from 2.39GHz to 2.52 GHz in lower frequency region and from 5.25 GHz to 5.54 GHz in higher frequency region. In applications, the bandwidths of both the frequency regions

TABLE II
 THE DEFINITIONS OF THE TWO FUNDAMENTAL CASES AND THE SIMULATED AND
 MEASURED RESULTS OF THE DUAL-BAND PATTERN RECONFIGURABLE ANTENNA WITH
 TWO-LAYER WALLS

	Switch	Case1	Case2
	S_{1a}, S_{1b}	Off	On
	S_{2a}, S_{2b}	Off	Off
	S_{3a}, S_{3b}	Off	Off
	S_{4a}, S_{4b}	Off	On
<i>Simulated peak gain direction</i>	2.45GHz	Omni	$\theta = -53^\circ$ $\phi = 225^\circ$
	5.25GHz	Omnilike	$\theta = -60^\circ$ $\phi = 225^\circ$
<i>Simulated peak gain (dBi)</i>	2.45GHz	0.50	6.17
	5.25GHz	5.73	9.24
<i>Measured peak gain direction</i>	2.45 GHz	Omni	$\theta = -73^\circ$ $\phi = 225^\circ$
	5.25 GHz	Omnilike	$\theta = -63^\circ$ $\phi = 225^\circ$
<i>Measured peak gain (dBi)</i>	2.45 GHz	0.23	5.85
	5.25 GHz	1.13	9.18

are enough. In Case 2, the -10 dB bandwidth is from 2.32 GHz to 2.5 GHz in lower frequency region and from 5.12 GHz to 5.48 GHz. Both of them accord with the specifications in these bands. Therefore, this dual-band coupling feeding antenna is a good candidate for use to reduce the complex matching circuits.

The measured patterns of Case 2, a directional case, and Case 1, an omni-directional case, at 2.45 GHz and 5.25 GHz are shown in Fig. 3.13 and Fig. 3.14, respectively. In Fig. 3.13(a), a directional pattern can be seen whose peak gain of 5.85 dBi at 2.45 GHz is

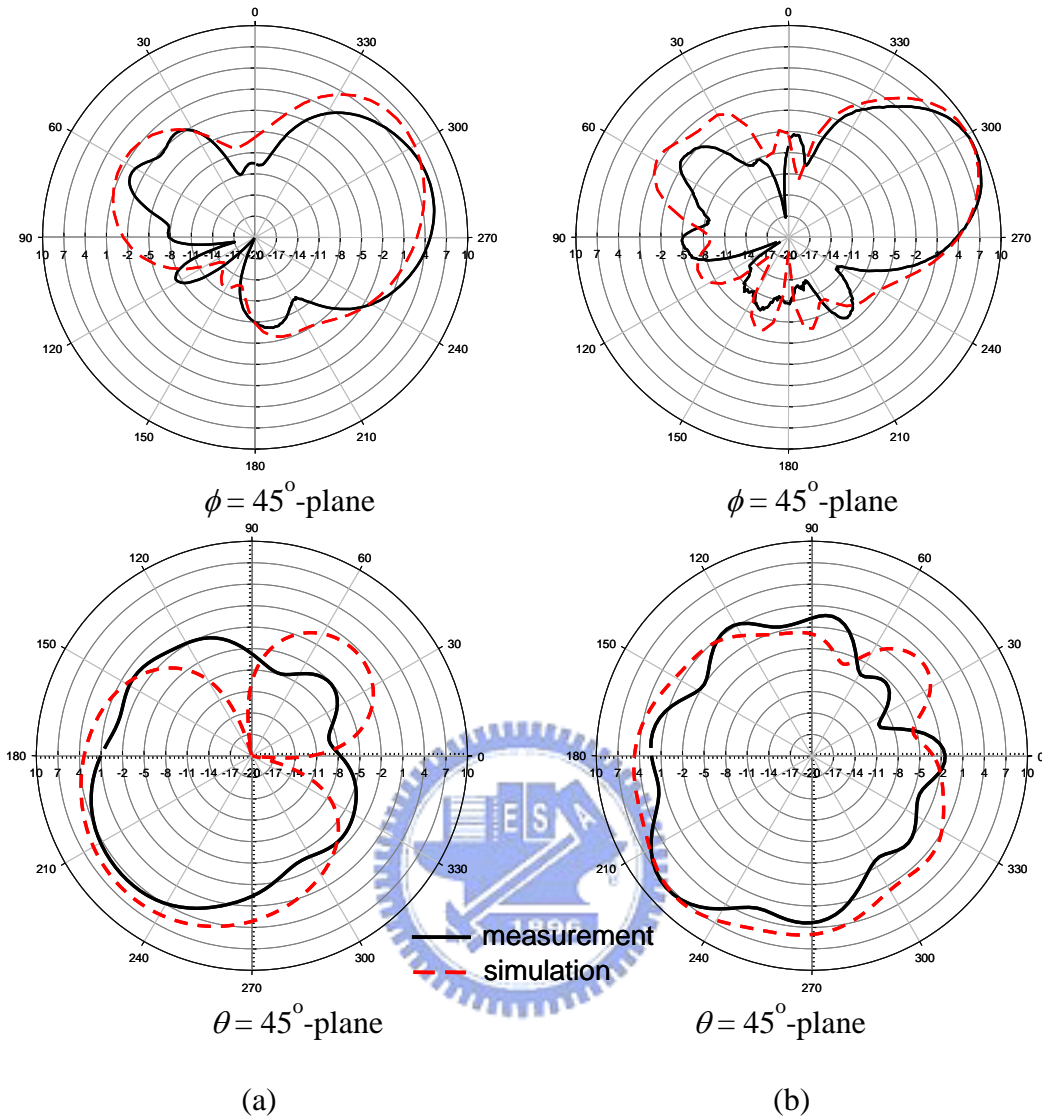


Fig. 3.13. The measured and simulated patterns of Case 2 at (a) 2.45 GHz (b) 5.25 GHz.

measured at $(\theta = -73^\circ, \phi = 225^\circ)$ with the side lobe level of 8.9 dB, while the peak gain of 9.18 dBi at 5.25 GHz is measured at $(\theta = -63^\circ, \phi = 225^\circ)$ with the side lobe level of 13.5 dB, as shown in Fig. 3.13(b). In addition, due to the beam tilting properties caused by the ground plane, the radiation patterns on $\theta = 45^\circ$ -plane are measured too. Apparently, the directional property toward where the switch states are off is good for use at both frequencies. The measured radiation patterns at $\phi = 45^\circ$ -plane coincide with the simulated ones at both frequencies. For Case 1, as shown in Fig. 3.14(a), the measured patterns at 2.45 GHz agree well with the simulated results in three different planes, $\theta = 45^\circ$ -, yz- and

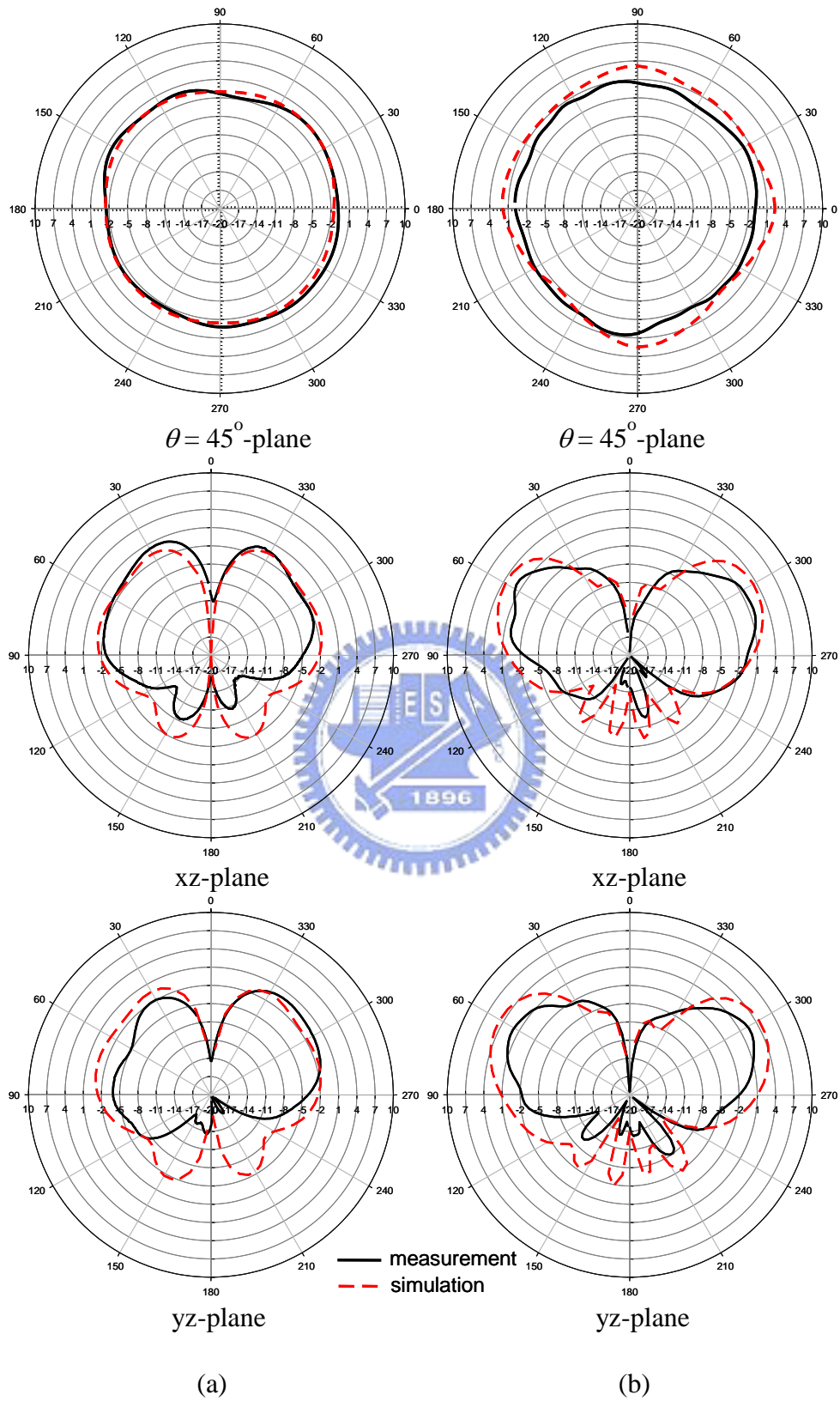


Fig. 3.14. The measured and simulated patterns of Case 1 at (a) 2.45 GHz (b) 5.25 GHz.

xz-plane. The peak gain is about 0 dB due to the effect of the pulling directors acted by the inner FSS walls. In Fig. 3.14(b), at 5.25 GHz, the measured radiation patterns are similar to the simulated patterns in $\theta = 45^\circ$ -, yz- and xz-plane, too. The maximum gain is 2.45 dB. At both frequencies, the variations of the patterns in $\theta = 45^\circ$ -plane are less than 3dB so good omni-directional patterns are obtained. In addition, because of the beam tilting property, the maximum gains are located within $-60^\circ < \theta < 60^\circ$. From above, it shows that both omni-directional and directional pattern are provided by this antenna.



Chapter 4 DUAL-BAND PATTERN RECONFIGURABLE ANTENNA WITH SINGLE-LAYER WALLS

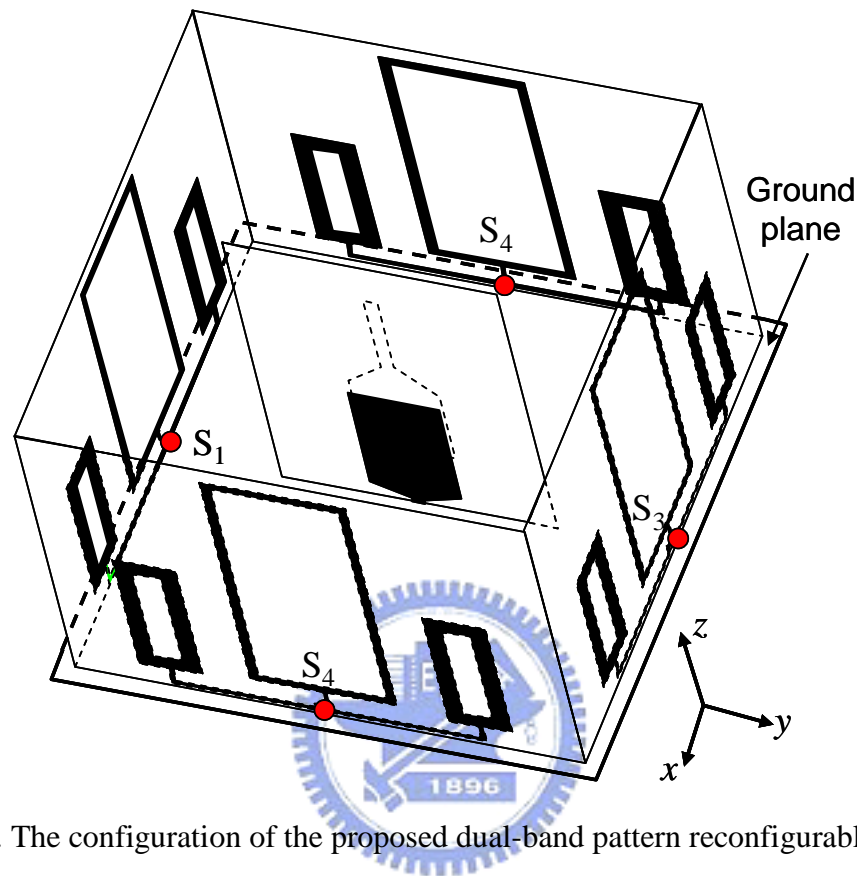


Fig. 4.1. The configuration of the proposed dual-band pattern reconfigurable antenna.

The size of the above design is determined by the wavelength of the lower frequency. Due to mounting the FSS walls on the ground, its size is $140 \text{ mm} \times 140 \text{ mm} \times 0.8 \text{ mm}$. This size is a little larger in the application for mobile devices. Therefore, we have to make it smaller if we plan to use it in mobile devices.

4-1 ANTENNA CONFIGURATION

The antenna configuration of this antenna is similar to the above one. It is made of a center dual-band feeding antenna, four rectangular walls and a finite ground, as shown in Fig. 4.1. Each wall has two groups of rectangular loops, which can reflect the vertically polarized incident electromagnetic waves when they resonate. The operating frequencies here are 2.45 GHz and 5.25 GHz. The properties of transmission and reflection of the loops are controlled by switches, whose names are $S_1 \sim S_4$, and horizontal and vertical metal control lines. On one switch state, both groups of rectangular loops are able to

resonate by excitement from vertically polarized incident wave. Therefore, they can reflect the waves. On the other switch state, those loops are disabled from resonance to look invisible for the vertically polarized incident waves. Only one switch is needed for usage on each wall, and it can reduce the cost of fabrication. Every switch is located at the intersection of the two control lines and the ground plate at the backside of the substrate of the wall. When the switch is transmissive, the center point of the horizontal control line and the end point of the vertical control line connect to the ground plate to form a short-circuit condition at those points. Contrarily, those points are isolated from the ground plate to be in an open-circuit condition when the switch is not threaded through.

The ground size is determined by the spacing between the driving element and the reflecting wall because those walls are vertically mounted on the ground plate. The ground size is quite smaller than the ground of the first proposed antenna because shorter spacing and the length of the walls. With dimension of $30 \text{ mm} \times 30 \text{ mm} \times 0.8 \text{ mm}$, the ground plane is fabricated on FR4 substrate with relative permittivity of 4.4.

A dual-band antenna is located at the center of the ground plate and designed for 2.45 GHz and 5.25 GHz. This antenna, which is perpendicular to the ground plate, is printed on the both side of the FR4 substrate with dimension of $40 \text{ mm} \times 30 \text{ mm} \times 0.8 \text{ mm}$. In addition, the matching circuit for the feeding antenna is printed on the other side of the substrate of the ground.

Moreover, the associate circuits for the switches can be fabricated under the ground plane, just like the first antenna. Therefore, the advantage that those circuits do not affect the properties of the antenna can be kept in this antenna. Designing circuits becomes easier because we can build our circuits without considering the influences on the antenna.

4-2 DESIGN PROCEDURE OF THE DUAL-BAND FSS WALLS

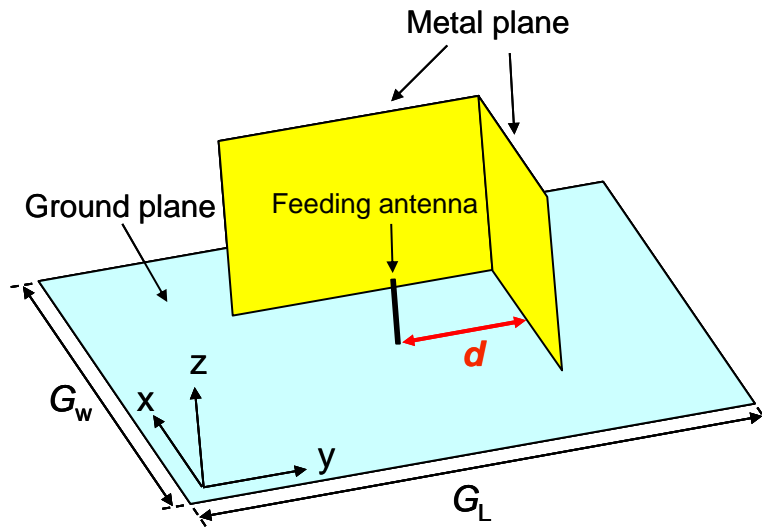


Fig. 4.2. The configuration of the proposed dual-band pattern reconfigurable antenna.

The proposed antenna is based on a corner reflector antenna. Therefore, the design idea of the wall is crucial. For a dual-band reflector wall, there are two major parts of designation: the spacing between the wall and the center feeding antenna and the switching reflector elements.

4-2-1 Spacing between the wall and the feeding antenna

According to the theory of a corner reflector antenna, the appropriate spacing between the wall and the driving element is from 0.25 times wavelength to 0.7 times wavelength, and the best one is 0.5 times wavelength among them. Therefore, the spacing for 2.45 GHz is between 30 mm and 85 mm while the spacing for 5.25 GHz is from 14 mm to 40 mm. The intersection of those two ranges is from 30 mm to 40 mm. Then we can find the best spacing.

In Fig. 4.2, a simulated method to determine the spacing is shown. Two metal planes with the width of 50 mm are mounted on the ground. The spacing between the wall and the driving element is defined as " d ". The length of these metal walls equal to twice the spacing between the wall and the driving element equals to twice the spacing between the wall and the driving element, which means that the length equals to $2d$. The dimension of ground plate, (G_w , G_L), is (140mm, 140 mm), which is enough to mount the metal walls

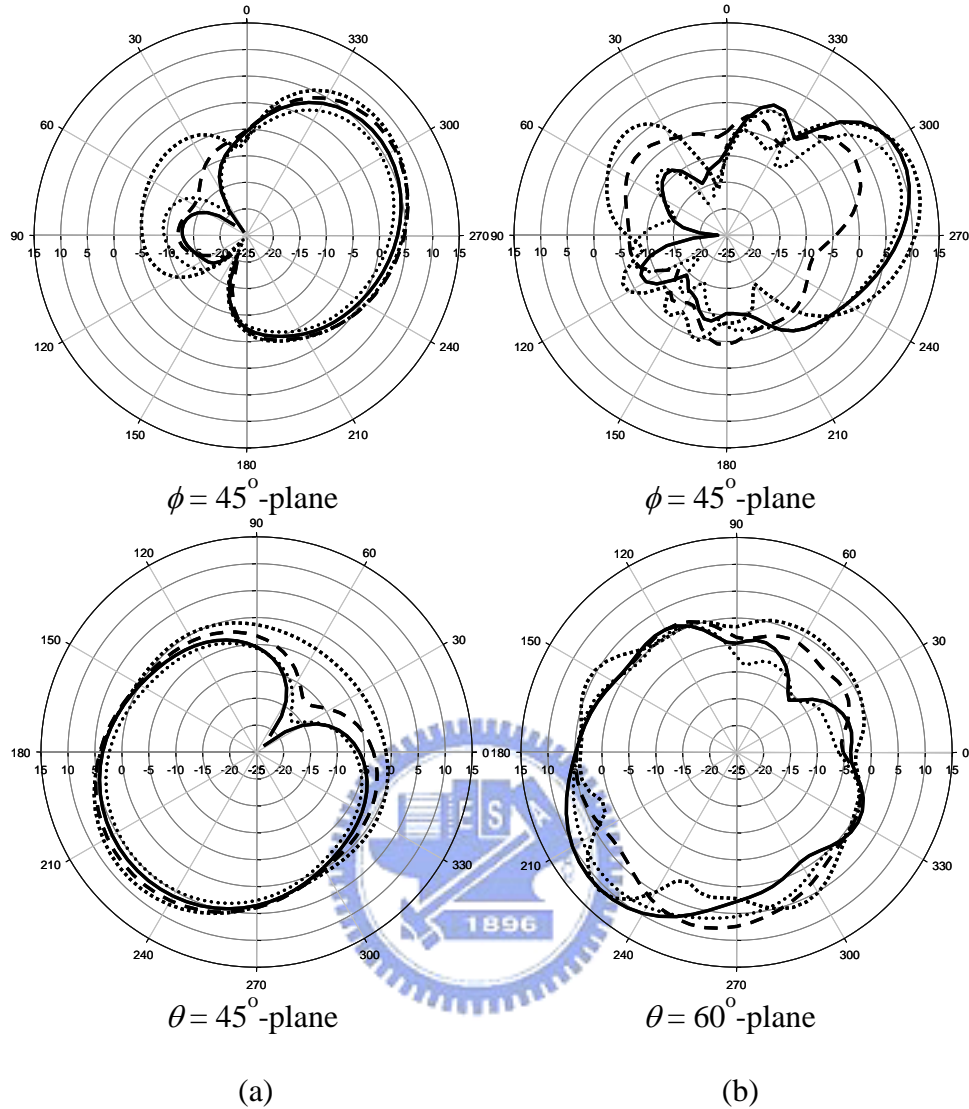


Fig. 4.3. The pattern variations for various spacing, d , (a) at 2.45 GHz (b) at 5.25 GHz.

when the spacing, d , is about 0.5 times wavelength at 2.45 GHz. The simulation results of the different spacing are shown in Fig. 4.3. As shown in Fig. 4.3(a), the maximum gain at 2.45 GHz does not vary too much but the backlobe when d varies so the patterns. In Fig. 4.3(b), the maximum gain at 5.25 GHz varies much with the variation of d . In addition, the shapes of patterns in $\theta = 45^\circ$ plane at 5.25 GHz change dramatically. The main beam diverges when $d = 60$ mm, even the maximum gain is enough, while some main beams have insufficient gains. Besides, the front-to-back ratio is an important parameter in a directional antenna. Therefore, considering the above conditions, the

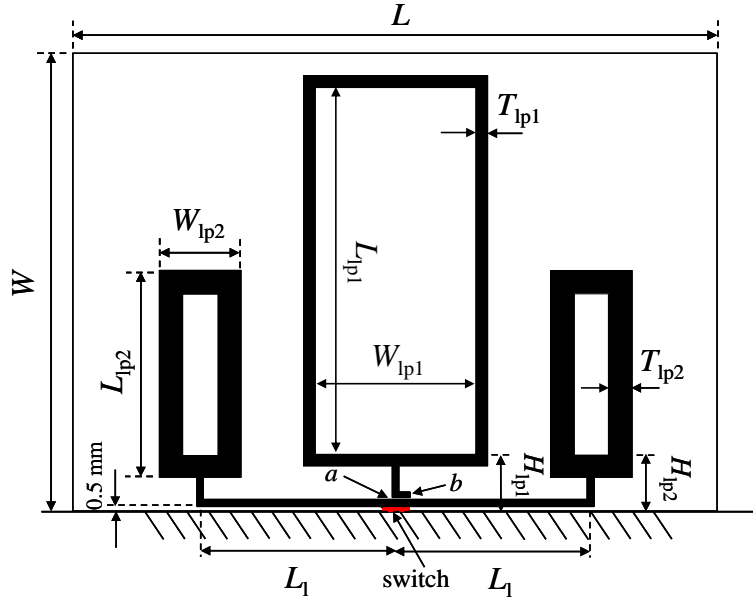


Fig. 4.4. The geometry of the switchable dual-band frequency selective surface.

spacing, $d = 28$ mm, is chosen, which has enough maximum gain, good shapes of patterns and sufficient front-to-back ratio.

4-2-2 Switching dual-band FSS elements

Now, let us consider the reflector elements on each wall. After the spacing between the wall and the driving element has been determined, the dimensions of the wall are obtained. As shown in Fig. 4.4, the circumference of the rectangular loop is about one wavelength of the operating frequency; moreover, the length of the rectangular loop must longer than the width due to the requirement of response on the vertically polarized electromagnetic waves. The length and width of the center loop, (L_{lp1}, W_{lp1}) , are 36 mm and 18 mm, respectively. Then, the length and width of the side loops, (L_{lp2}, W_{lp2}) , are 18 mm and 7mm, respectively. The center larger loop operates at 2.45 GHz, and the two side loops are responsible for 5.25 GHz. The current distribution on those reflectors changes with the switch states, so their frequency responses are quite different. Besides, there is a small spacing between the vertical line and horizontal line. This results from the unwanted interaction between them when they are connected together. It will be discussed later. The points, a and b , connect the center point of the horizontal line and the end point of the vertical line with a switch mounted on the backside of the wall.

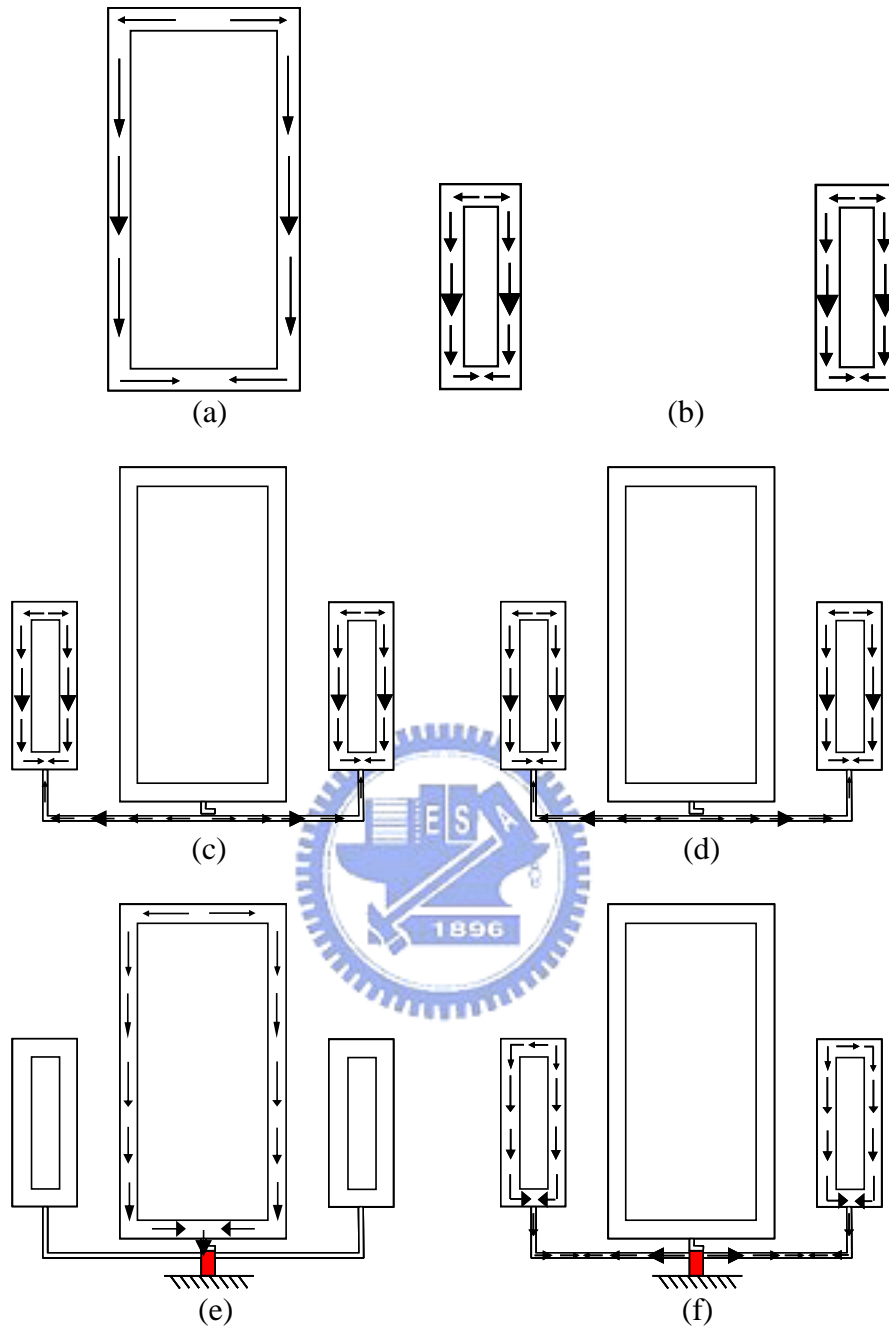


Fig. 4.5. The induced current distribution on the reflecting loops (a) at 2.45 GHz. (b) at 5.25 GHz. (c) at 2.45 GHz (d) at 5.25 GHz when the switch is impassible. (e) at 2.45 GHz (f) at 5.25 GHz when the switch is passable.

In the beginning, consider about a single center large rectangular loop and two side rectangular loops without the transmission lines. As shown in Fig. 4.5(a), due to the symmetry of the center loop and about one-wavelength circumference of the loop, resonant current nulls appear at the top and bottom center of the loop, and the peak

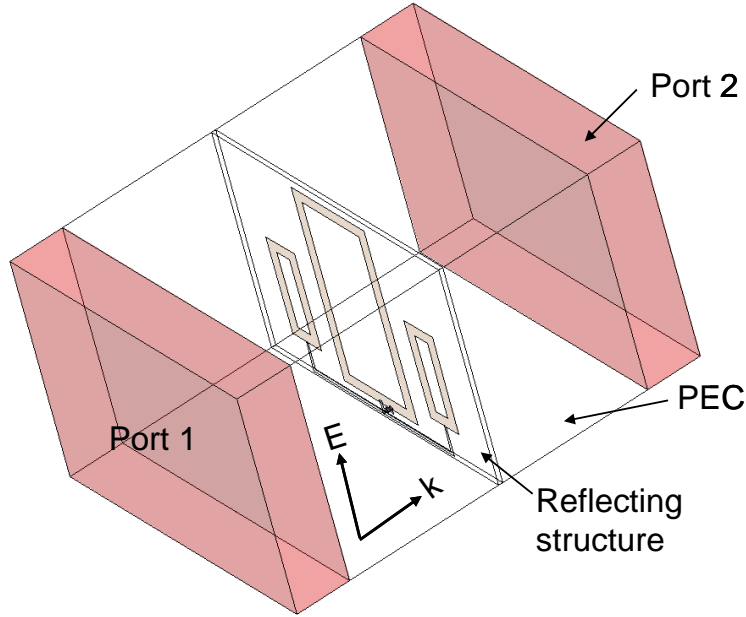
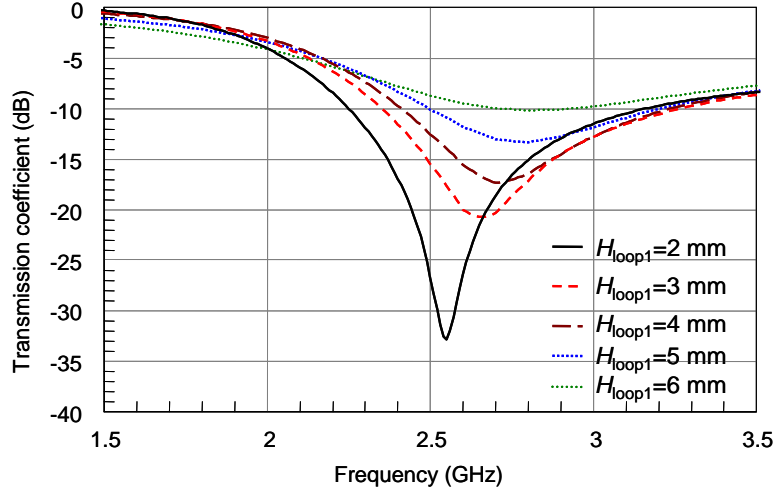


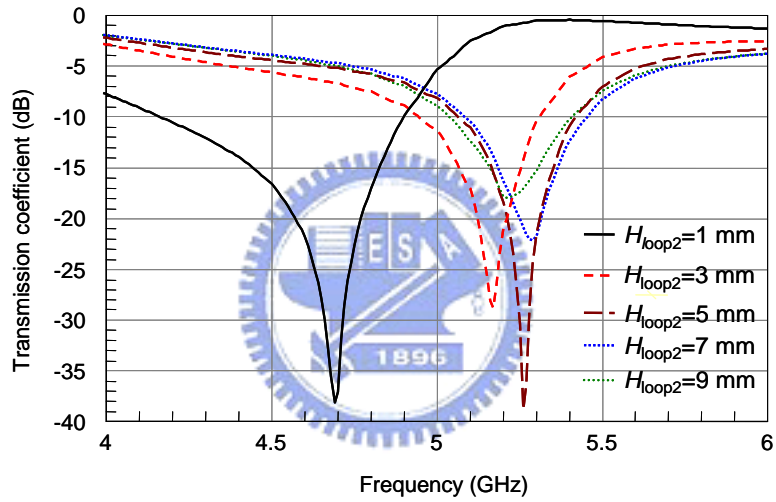
Fig. 4.6. The simulation model for designing dual-band switchable FSS structures.

current shows at the center of the arms at both side. Then, the re-radiated fields excited from the resonant current would cancel the incoming waves at the backside of the reflector while generate a wave propagating toward the opposite direction. Hence, the reflector reflects the incident waves. For 5.25 GHz, as shown in Fig. 4.5(b), the operating principle is the same as mentioned.

Next, let us think that two control lines exist in our schematics. Consider the control line for 2.45 GHz first. As shown in Fig. 4.5(c), a short control line connects the bottom middle point of the center loop. When the vertically polarized waves are incident, an open-circuit condition shows at the end of the line if the switch is impassible. In comparison with the wavelength of 2.45 GHz, its length is quite short. As a result, a nearly open-circuit condition appears at the bottom center point of the loop, which keeps the resonant current distribution. Hence, the center loop can reflect the vertically polarized incident waves as the one without the control line. For 5.25 GHz, due to the goal that reflectors for both frequencies can be controlled simultaneously, an open-circuit should exist at both ends of the horizontal control line when the switch is impassible. Due to symmetry of the line, open-circuit would appear at the middle point of the line. A one-wavelength of 5.25 GHz transmission line is needed here. According to the transmission line theory [25], through the half-wavelength transmission line from the midpoint of the



(a)



(b)

Fig. 4.7. The transmission coefficient curves of the reflectors for various heights of (a) the center loop (b) two side loops.

line to one of the ends, the induced current can be remained, as shown in Fig. 4.5(d), so the property of reflection at 5.25 GHz can exist.

On the other hand, when the switch is passable, a short-circuit condition exists at the end of the vertical control line and the midpoint of the horizontal control line. Therefore, a nearly short-circuit condition shows at the bottom center point of the center loop, and it shows at both ends of the horizontal line by a half-wavelength of 5.25 GHz transmission line. Therefore, the current distributions are destroyed, as shown in Fig. 4.5(e)(f). The levels of the induced current become weak so that the re-radiated field from them can be ignored. As a result, the incoming waves can pass through the FSS structures.

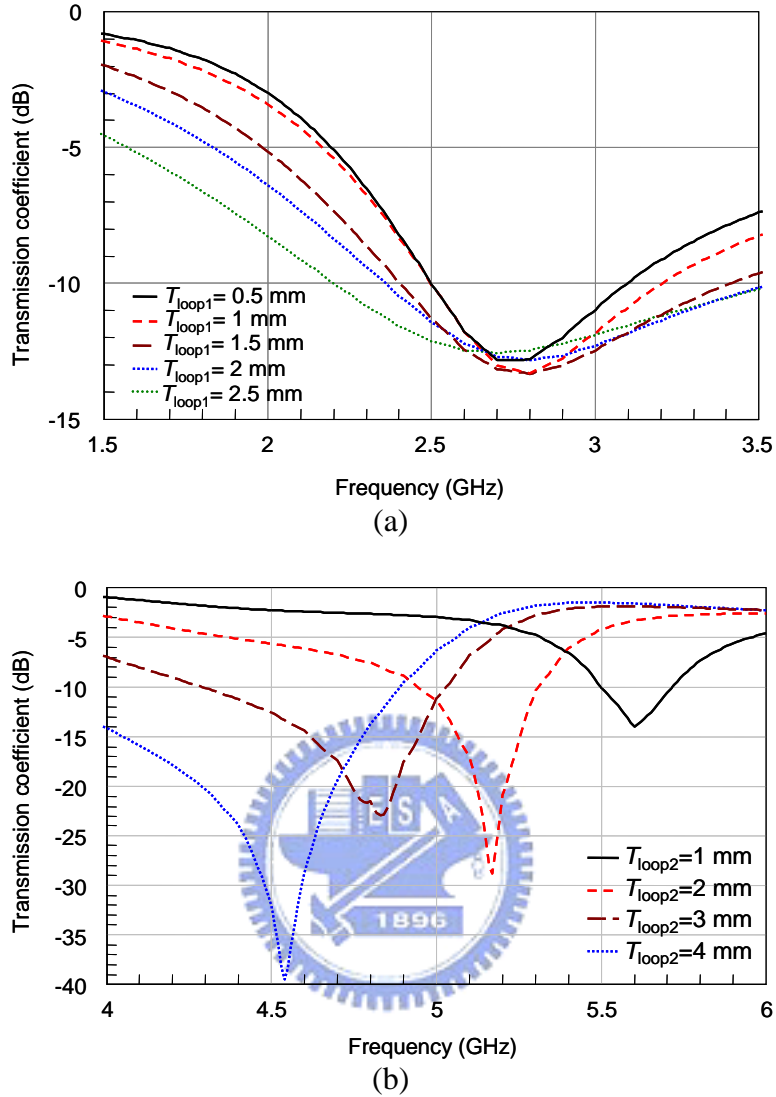


Fig. 4.8. The transmission coefficient curves of the reflectors for various thickness of (a) the center loop (b) two side loops.

The full-wave electromagnetic software Ansoft HFSS [26] was employed to analyze this switching reflector structures. The simulated method is shown in Fig. 4.6. Two ports excite the vertical polarized electromagnetic waves which are incident to the reflectors at the center. The boundary conditions around the structure are the perfect conducting surface under the reflector to be the ground and the radiation boundary at the other three surfaces to make it close to the conditions of the final proposed antenna. First, we define the transmission coefficient (S_{21}) of the situation of no any reflector at the center as the reference. Then, we simulate the transmission coefficient with reflectors and subtract the reference from it to get the transmission coefficients of reflectors. There are some

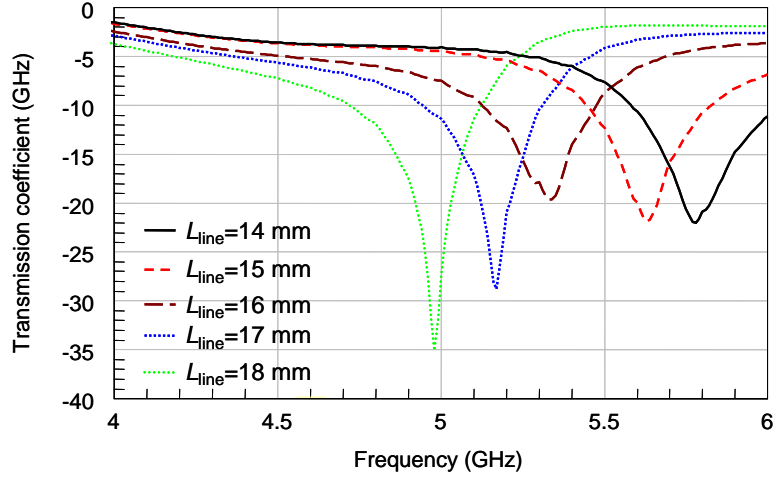


Fig. 4.9. The transmission coefficient curves of the reflectors for various horizontal position respect to the center point of the wall of two side loops.

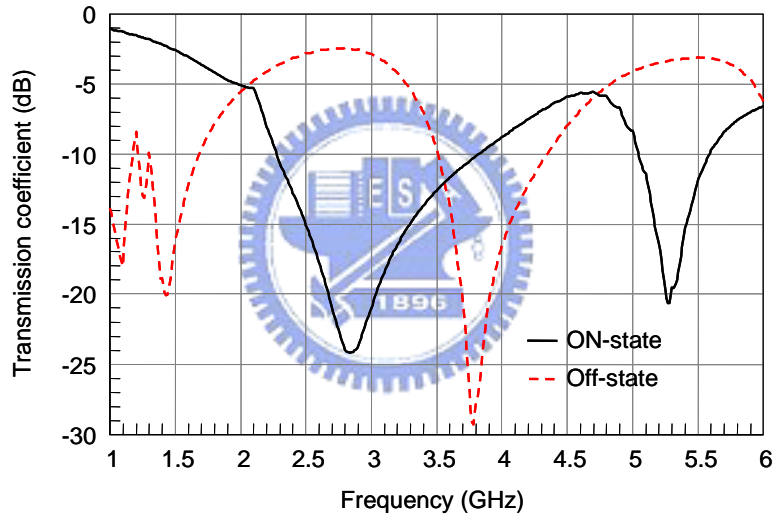


Fig. 4.10. The transmission coefficient of the proposed reflector in ON-state and Off-state.

parameters except the dimensions of the loops can affect the operating frequencies and the bandwidth. As shown in Fig. 4.7, the heights, H_{lp1} of the center loop and H_{lp2} of the two side loops, vary with $T_{lp1} = 1$ mm and $T_{lp2} = 2$ mm. The resonance frequencies increase with increment of heights of the loops. Because the operating frequencies are 2.45 GHz and 5.25 GHz, H_{lp1} and H_{lp2} are chosen from 2 mm to 5mm and from 3mm to 9mm, respectively. In Fig. 4.8, the influences of the thickness of the loops are shown. For 2.45 GHz, T_{lp1} does not affect the resonant frequency but the bandwidth in Fig. 4.8(a). Nevertheless, the influence of T_{lp2} is severe. The resonant frequency goes lower when the thickness increases, but the bandwidth increases, as shown in Fig. 4.8(b). In addition,

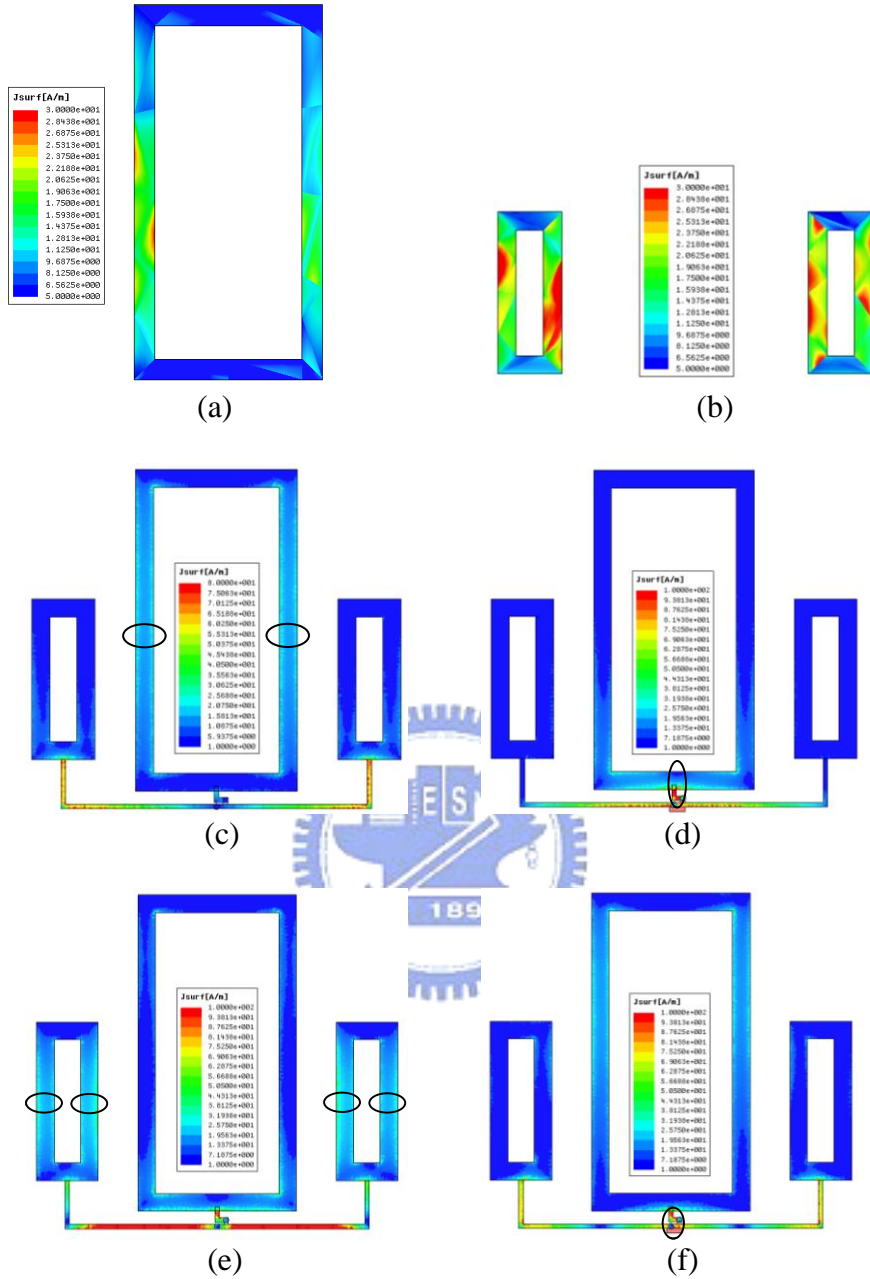
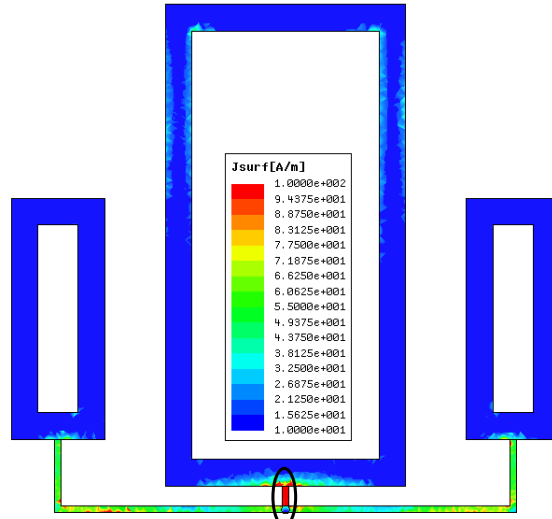
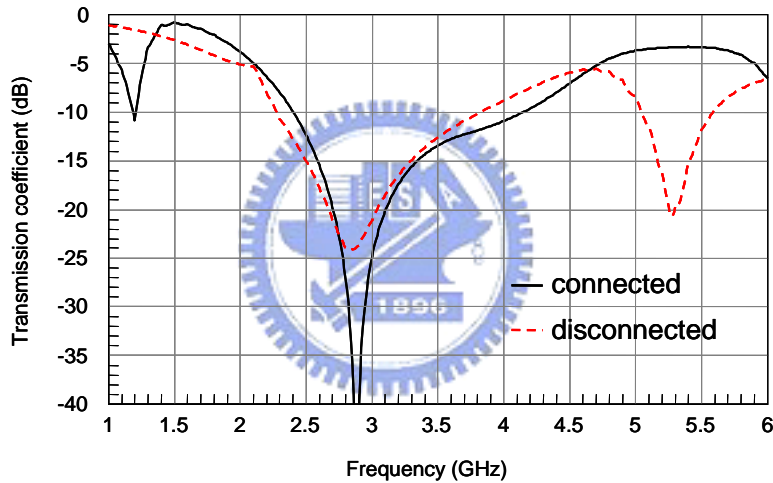


Fig. 4.11. The simulated current distribution on the reflecting loops (a) at 2.45 GHz. (b) at 5.25 GHz. (c) at 2.45 GHz in ON-state. (d) at 2.45 GHz in Off-state. (e) at 5.25 GHz in ON-state. (f) at 5.25 GHz in Off-state.

there is one more parameter for 5.25 GHz to be discussed. The variation of the horizontal distance from the center point of the wall, L_1 , is shown in Fig. 4.9. The resonant frequency decreases with increment of L_1 . Based on the design frequency of 5.25 GHz, the alternative range is between 16 mm and 17 mm. According to the above parameter studies and the consideration of a half-wavelength of 5.25 GHz control line, (H_{lp1}, T_{lp1})



(a)



(b)

Fig. 4.12. (a) The simulated current distribution at 5.25 GHz when two transmission line connects. (b) The transmission coefficient curves when two transmission lines connect or disconnect.

are (4.5 mm, 2 mm) for the center rectangular loop, and (H_{lp2}, T_{lp2}, L_1) are (6 mm, 2 mm, 17 mm). The transmission coefficient of the final reflector wall is shown in Fig. 4.10. ‘ON-state’ means that the FSSs can reflect waves while ‘Off-state’ means that the FSSs look transparent to waves. The transmission coefficients at both frequencies in On-state are lower than -10 dB while those in Off-state are higher than -3 dB. Therefore, good transmission in ON-state and good reflection in Off-state can be achieved.

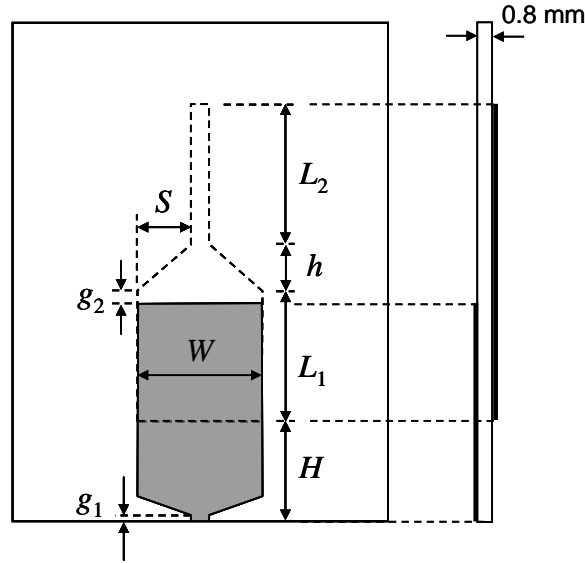


Fig. 4.13. The geometry of the dual-band feeding antenna.

The simulated current distributions excited by vertically polarized electromagnetic waves at both operating frequencies are shown in Fig. 4.11. The current distribution without control lines are shown in Fig. 4.11(a) as references for reflecting waves. Even though open-circuit does not really show up at the both end of the control lines due to the coupling effect, the current distributions in on-state in Fig. 4.11(c) and (e) are still similar to references to keep good resonances. Compared to them, the current level and distribution in off-state are different, as shown in Fig. 4.11(d) and (f). Therefore, good transmission in on-state and good reflection in off-state can be obtained.

In addition, the transmission lines for 2.45 GHz and 5.25 GHz cannot connect together because the center larger loop provides short-circuit condition to the horizontal transmission line, as shown in Fig. 4.12. In Fig. 4.12(a), the strong current distribution occurs at the center point of the horizontal line so the current distribution on the loops will be destroyed, just like the switch is passable. In Fig. 4.12(b), we can see that the S_{21} at 5.25 GHz is higher than -3 dB so the property of reflection at 5.25 GHz is cancelled. As a result, a double-pole-double-throw (DPDT) switch is needed in this antenna application to separate two transmission lines and to control them simultaneously.

4-2-3 Design of the feeding antenna

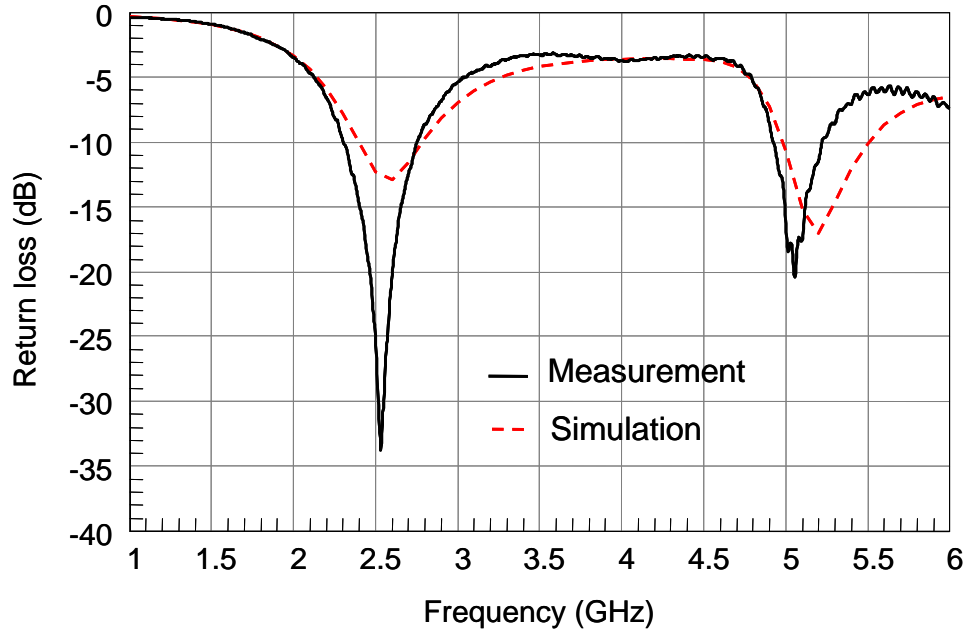


Fig. 4.14. The measured and simulated return loss of the dual-band feeding antenna.

As mentioned in Chapter 3, using a coupling effect to design our feeding antenna is a good design method to make the impedance matching at different cases easier. The proposed feeding antenna is shown in Fig. 4.13. The parameters of the back part, (H, h, L_1, L_2, S, g_2), are (4 mm, 3.75 mm, 8.5 mm, 11.25 mm, 4.25 mm, 0 mm), and the parameters of the front part, (W, g_1), are (10 mm, 2 mm). The whole length of the front part is 14.5 mm, which is about quarter wavelength of 5.25 GHz, and the whole height of the back part is 29.5 mm, which is about quarter wavelength of 2.45 GHz. By adjusting the gap, g_1 , can get a good matching at 5.25 GHz. The coupling effect can be adjusted by L_1 and g_2 , which control the intersected area between the front and back part. The measured and simulated results are shown in Fig. 4.14. In lower frequency band, the measured bandwidth that return loss is lower than -10 dB is from 2.3 GHz to 2.75 GHz while the simulated bandwidth is from 2.4 GHz and 2.79 GHz. In higher frequency band, the measured bandwidth is between 4.92 GHz and 5.22 GHz while the simulated one is between 4.98 GHz and 5.50 GHz. A little frequency shift occurs in higher frequency band, and it may be caused by fabrication.

4-3 MEASUREMENT RESULTS

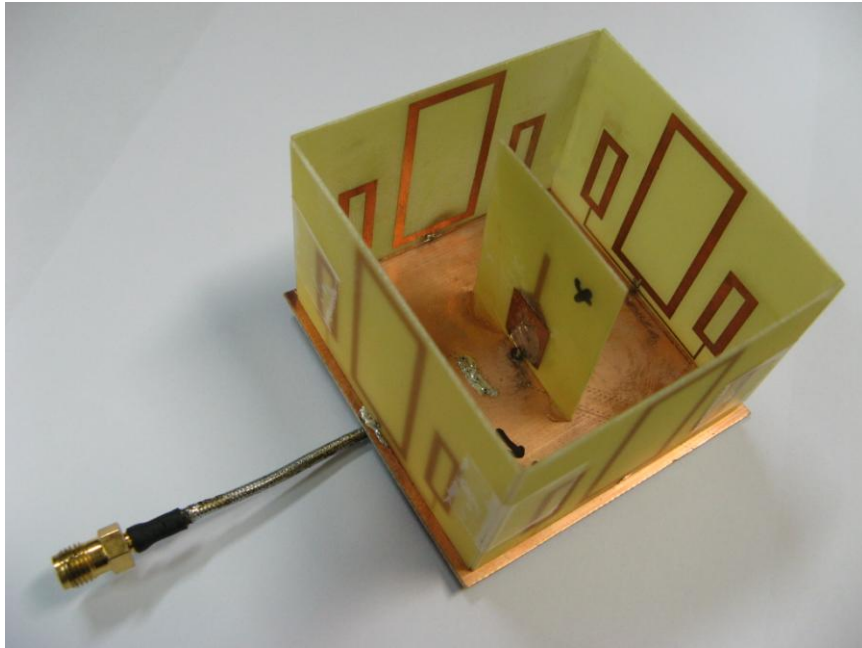


Fig. 4.15. The photo of the realized dual-band pattern reconfigurable antenna

The realized dual-band pattern reconfigurable antenna is shown in Fig. 4.15. We use idea open and short circuit as two different switch states. ‘Case 1’ is the case with the omni-directional pattern when the switches are on while ‘Case 2’ is the case with the directional patterns when only two adjacent switches are on. We only focus on these two cases because they are the most widely used in applications. The definition of each case and the simulated and measured results are listed in TABLE III. The measured return losses in Case 1 and Case 2 are shown in Fig. 4.16. Both operating frequencies are resonant in both cases. Both of them are good enough for use and observing the pattern switching.

The measured radiation patterns in Case 2 and Case 1 are shown in Fig. 4.17 and Fig. 4.18, respectively. In Case 2, a directional pattern is provided, as shown in Fig. 4.17. The maximum gain at 2.55 GHz is 3.54 dBi at $\phi = 225^\circ$ and $\theta = -65^\circ$, and that at 5.25 GHz is 7.77 dBi at $\phi = 225^\circ$ and $\theta = -30^\circ$. Moreover, their front-to-back (FTB) ratios are important parameters. At 2.55 GHz, the FTB ratio is 8.31 dB, and the FTB ratio is 9.74 at 5.25 GHz. Both of them are good enough to enhance the desired signals and minimize the unwanted signals. In Fig. 4.18, omni-directional patterns at both frequencies in Case 1 are

TABLE III
 THE DEFINITIONS OF THE TWO FUNDAMENTAL CASES AND THE SIMULATED AND
 MEASURED RESULTS OF THE DUAL-BAND PATTERN RECONFIGURABLE ANTENNA WITH
 SINGLE-LAYER WALLS

	Switch		Case1	Case2
	S ₁		On	On
	S ₂		On	On
	S ₃		On	Off
	S ₄		On	Off
<i>Simulated peak gain direction</i>	2.55GHz		Omni	$\theta = -65^\circ$ $\phi = 225^\circ$
	5.25GHz		Omnilike	$\theta = -40^\circ$ $\phi = 225^\circ$
<i>Simulated peak gain (dBi)</i>	2.55GHz		2.01	4.27
	5.25GHz		4.3	7.81
<i>Measured peak gain direction</i>	2.55 GHz		Omnilike	$\theta = -45^\circ$ $\phi = 225^\circ$
	5.25 GHz		Omnilike	$\theta = -30^\circ$ $\phi = 225^\circ$
<i>Measured peak gain (dBi)</i>	2.55 GHz		2.08	3.54
	5.25 GHz		4.67	7.77

shown. The omni-directional patterns are formed within $-60^\circ < \theta < 60^\circ$ due to the ground effect. In xz- and yz-plane at 2.45 GHz, the patterns at $\theta = 60^\circ$ are around 2 dB, and at 5.25 GHz, the patterns at $\theta = 45^\circ$ are about 4.5 dB. Therefore, omni-directional patterns are achieved. In addition, the patterns in xy-plane at both cases do not show because of the unwanted interference from the ground plane. As a result, the radiation patterns at xy-plane are meaningless. The measured results coincide with the simulated ones well. In

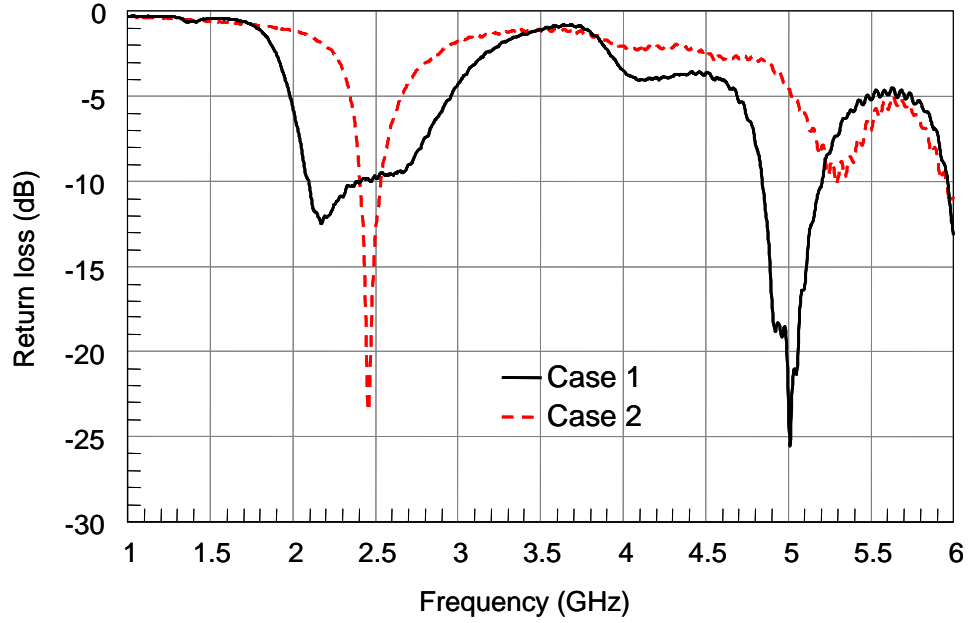


Fig. 4.16. The measured return losses in Case 1 and Case 2.

conclusion, both the directional patterns and the omni-directional patterns at both frequency bands can be provided with this proposed antenna.



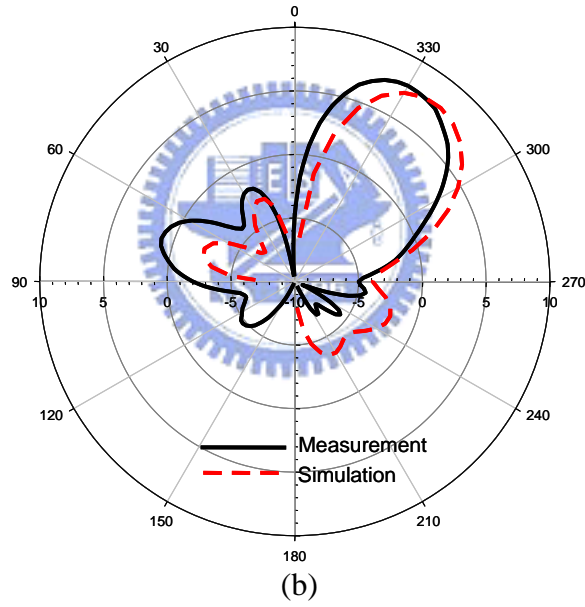
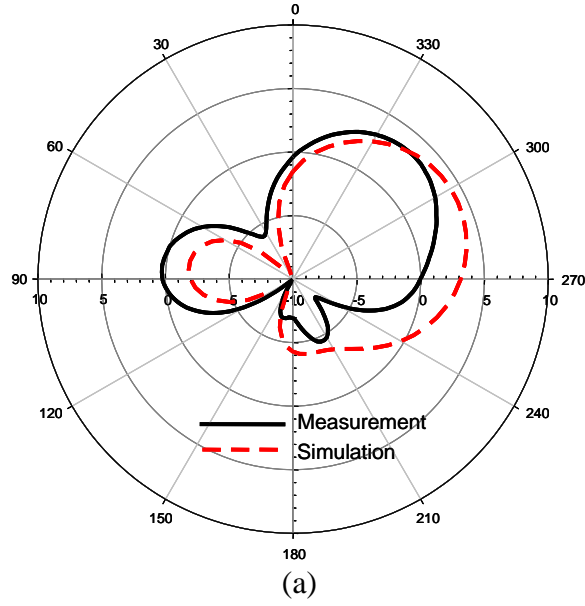


Fig. 4.17. The measured and simulated radiation patterns in $\phi = 45^\circ$ -plane in Case 2 at (a) 2.55 GHz. (b) 5.25 GHz.

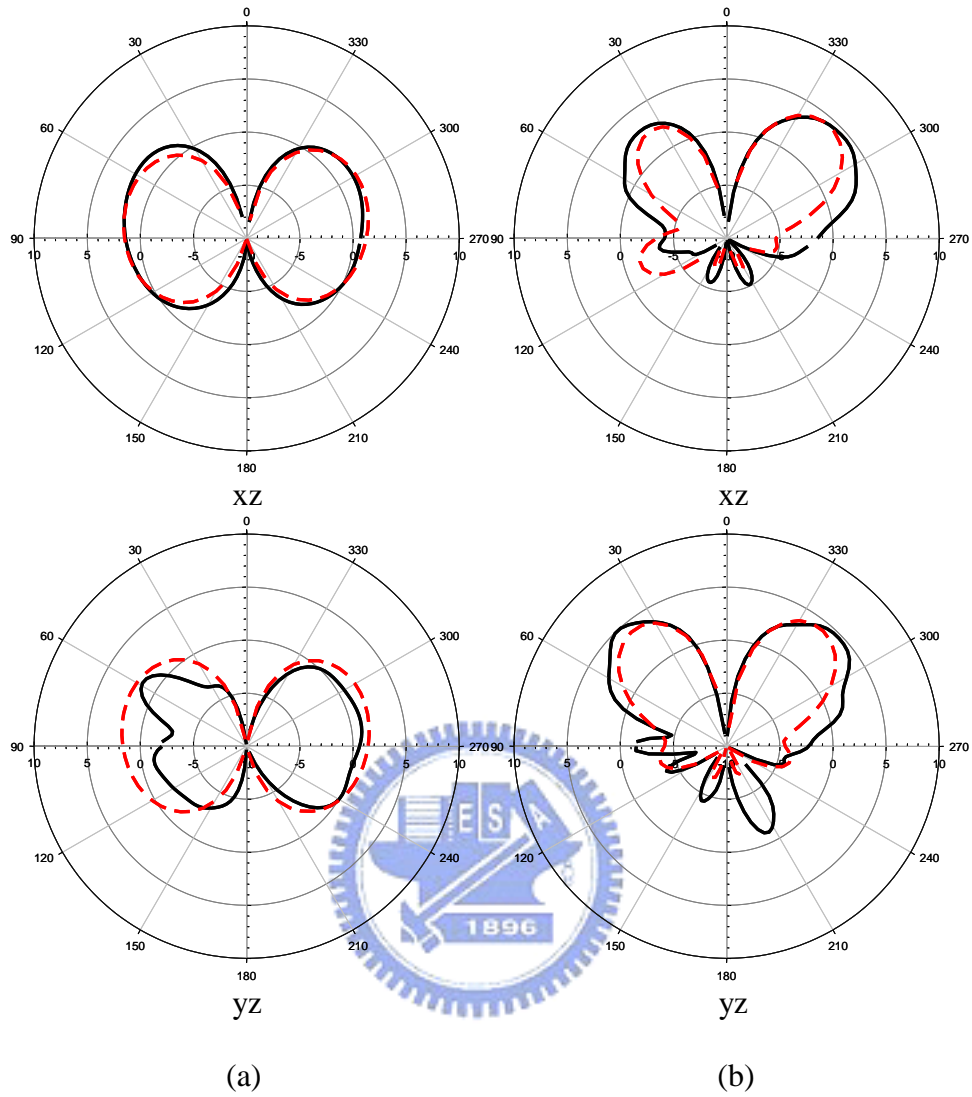


Fig. 4.18. The measured and simulated radiation patterns in xz - and yz -plane in Case 1 at (a) 2.55 GHz. (b) 5.25 GHz.

Chapter 5 DUAL-BAND PATTERN RECONFIGURABLE ANTENNA BY FOUR SWITCHING RECTANGULAR LOOPS

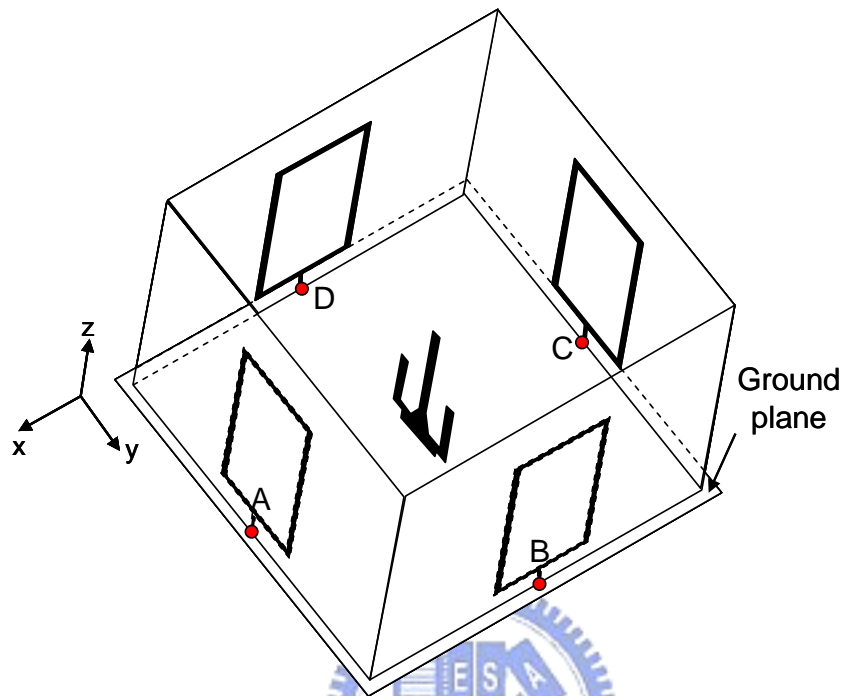


Fig. 5.1. The configuration of the proposed dual-band pattern reconfigurable antenna.

A much easier structure to operate as a dual-band reflector is introduced in this chapter. It is modified from the second dual-band reflector in the Chapter 4 in this thesis. This new structure has the almost the same properties as the second one. Besides, this antenna uses four switches on the four walls, respectively. The switches used here can be the simple one such as pin diodes and MEMS.

5-1 ANTENNA CONFIGURATION

As shown in Fig. 5.1, this simple dual-band pattern reconfigurable reflector antenna consists of a simple dual-band feeding antenna at the center, four reflecting sidewalls with rectangular loops and a finite ground with the same dimensions as the ground dimension of the second proposed antenna. The reason that both ground sizes are the same is that the same conditions are required, so the spacing between the wall and the feeding element is 28 mm and the length of the wall is 56 mm. Then the ground size is 30 mm \times 30 mm \times 0.8 mm. On each wall, there are a simple rectangular loop, a short

vertical control line and a switch. A, B, C, and D are the symbols for the switches on each wall, which is between the lower end of the vertical control line. The properties of transmission and reflection of the wall are controlled by the switch states. On one switch states, the wall with a rectangular loop works as a reflector to block the incident electromagnetic waves. On the other switch state, it becomes invisible for the incident waves so the waves can go through this wall unchangingly. The matching circuits for the feeding dual-band antenna and the associate circuits for switches can be fabricated on the other side of the ground plane to prevent unwanted influences on the electromagnetic fields of the proposed antenna. Unlike the second proposed antenna, the switches used here are simple compared to the Double Pole Double Throw (DPDT) used in the second antenna. Therefore, this dual-band pattern reconfigurable antenna with a simple structure and simple switches is a better candidate for applications nowadays.



5-2 DESIGN OF DUAL-BAND PATTERN RECONFIGURABLE STRUCTURES WITH A SINGLE LOOP

5-2-1 Design of the reflector by a single loop

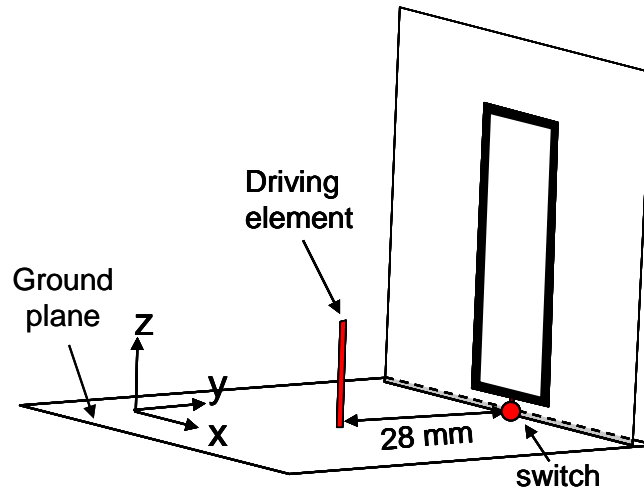


Fig. 5.2. The configuration of the simulated assignment.

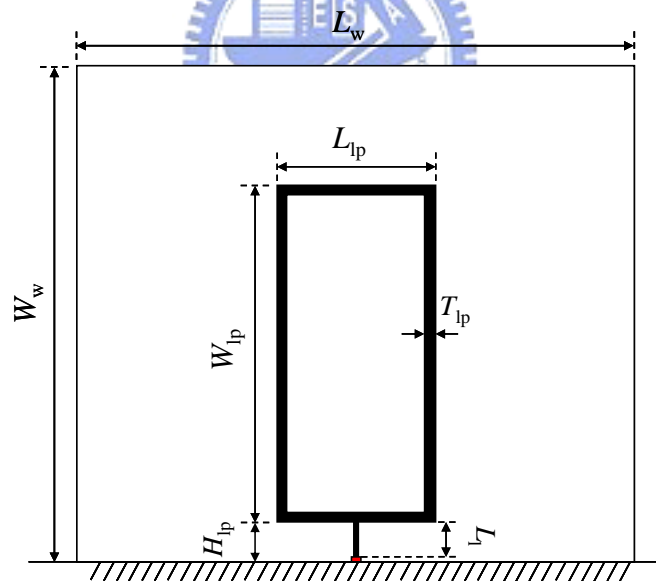


Fig. 5.3. The geometry of the dual-band switching reflector.

The simulated method of reflectors is shown in Fig. 5.2. A driving element for 2.45 GHz or 5.25 GHz is located at the center of the ground plane. A wall with a single rectangular loop and a short control line is built in positive y direction, and a switch is fabricated between the end of the vertical control line and the ground plane. The spacing

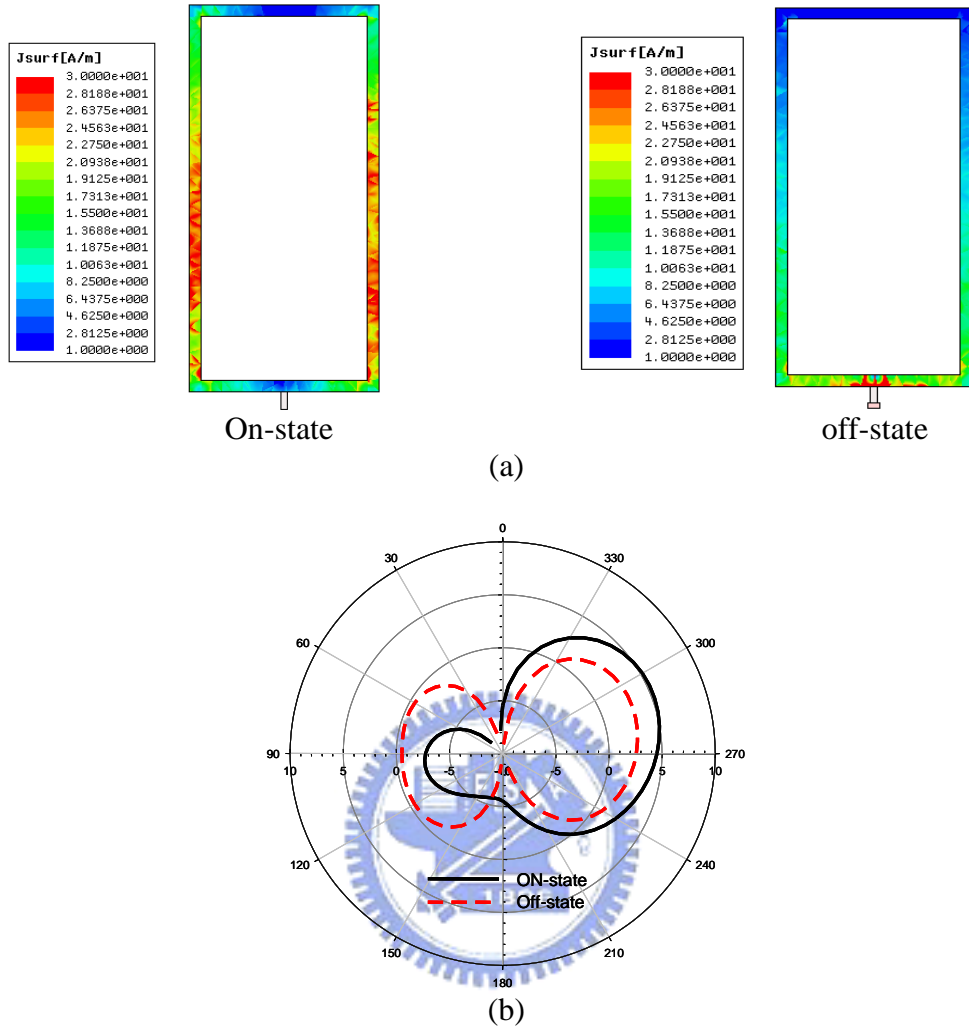


Fig. 5.4. (a) The current distribution on the loop in on- and off-state at 2.45 GHz. (b) The radiation patterns in ON- and Off-state at 2.45 GHz.

between the driving element and the wall has been determined in Chapter 4-2-1. For a switching reflector for 2.45 GHz, the circumference of the loop should be around one wavelength of 2.45 GHz. The operating principle at 2.45 GHz for reflecting vertically polarized incident waves is quite the same as mentioned in Chapter 3 and 4. Basically, this loop only responses at 2.45 GHz. Nevertheless, if we can excite strong resonant current of 5.25 GHz on the vertical arms, this structure can reflect vertically polarized incident waves of 5.25 GHz, too.

After some simulations, a dual-band rectangular loop is obtained. The geometry of the loop is shown in Fig. 5.3. $(L_w, W_w) = (28 \text{ mm}, 50 \text{ mm})$ is determined when the best spacing for dual-band reflection is decided. The other parameters of this geometry, $(L_{lp},$

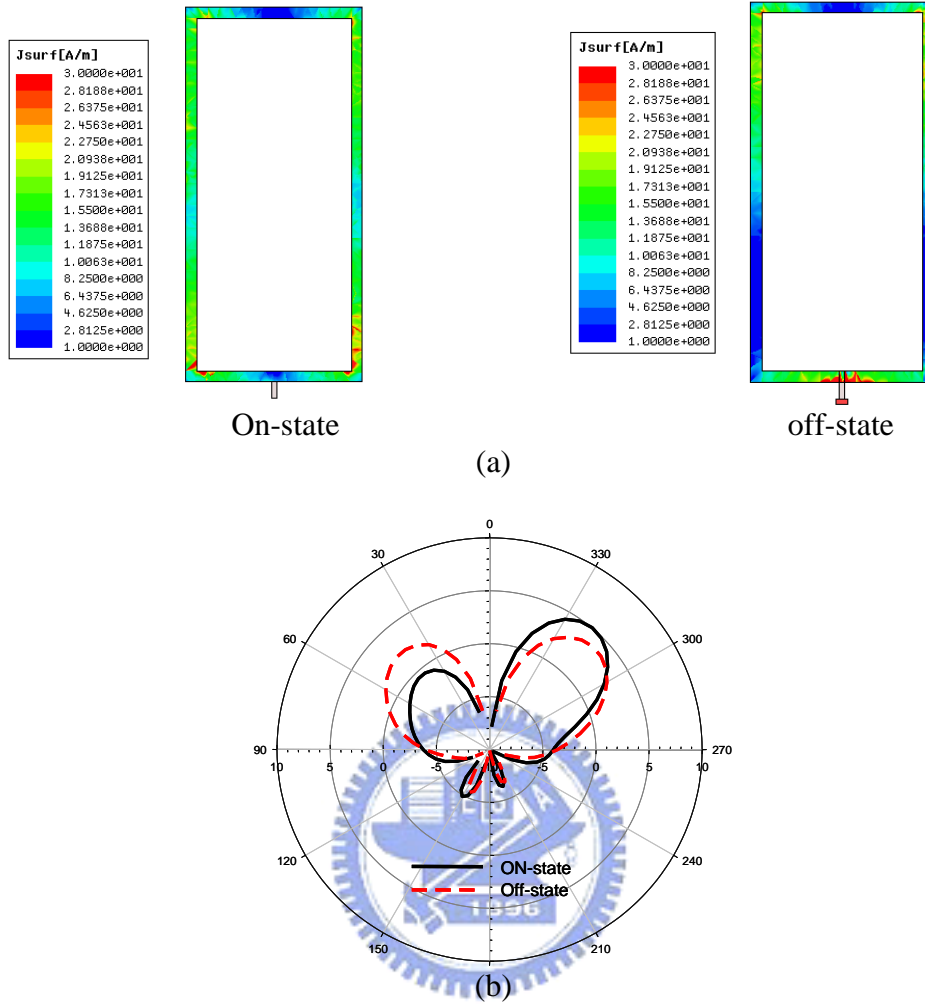


Fig. 5.5. (a) The current distribution on the loop in on- and off-state at 5.25 GHz. (b) The radiation patterns in ON- and Off-state at 5.25 GHz.

W_{lp} , T_{lp} , H_{lp} , L_1), are 34 mm, 16 mm, 1 mm, 4 mm and 3.5 mm, respectively. The simulated current distribution and radiation patterns in both on- and off-state at 2.45 GHz are shown in Fig. 5.4. In Fig. 5.4(a), when the switch is impassable, two current nulls appear at the center of the top and bottom horizontal arms due to symmetry. In addition, due to one-wavelength of 2.45 GHz circumference, strong current is excited at the center of two vertical arms. Therefore, the vertically polarized incident waves of 2.45 GHz are reflected. When the switch connects the vertical line with the ground plane, however, a short-circuit condition shows at the midpoint of the bottom horizontal arm. The induced current distributions on the vertical arms are destroyed so that the level becomes weak. The property of reflection becomes weak too, as shown in Fig. 5.4(b). Now, consider the

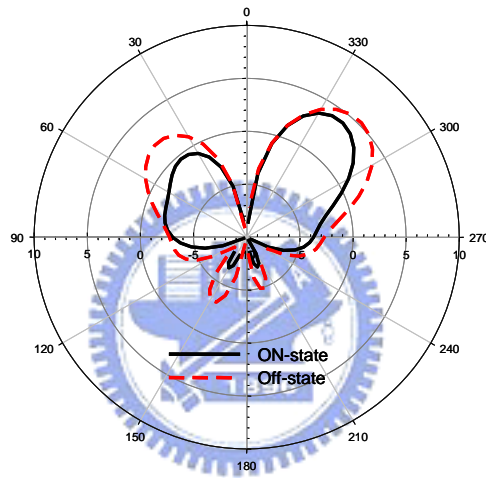
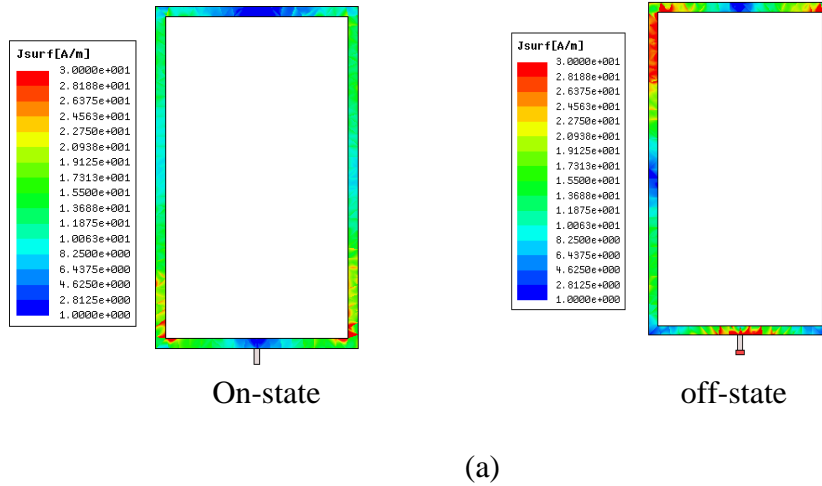


Fig. 5.6. The effects of the increment of the width, W_{lp} . (a) The current distribution on the loop in ON- and Off-state at 5.25 GHz. (b) The radiation patterns in on- and off-state at 5.25 GHz.

situations as shown in Fig. 5.5(a). A two-wavelength resonance of 5.25 GHz occurs with four current nulls at the midpoint of each arm when the switch is impassable. Here, we have to focus on the location of the strong current. The strong current occurs mostly on the vertical arms so that the vertically polarized incident waves of 5.25 GHz can be reflected effectively. However, when the switch is passable, the resonant current distribution of 5.25 GHz at 5.25 GHz also appears, but it is a three-quarter-wavelength resonance. One of the strong current appears at the bottom horizontal arm, whose radiated field is cancelled by the current on the ground. Only the strong current on

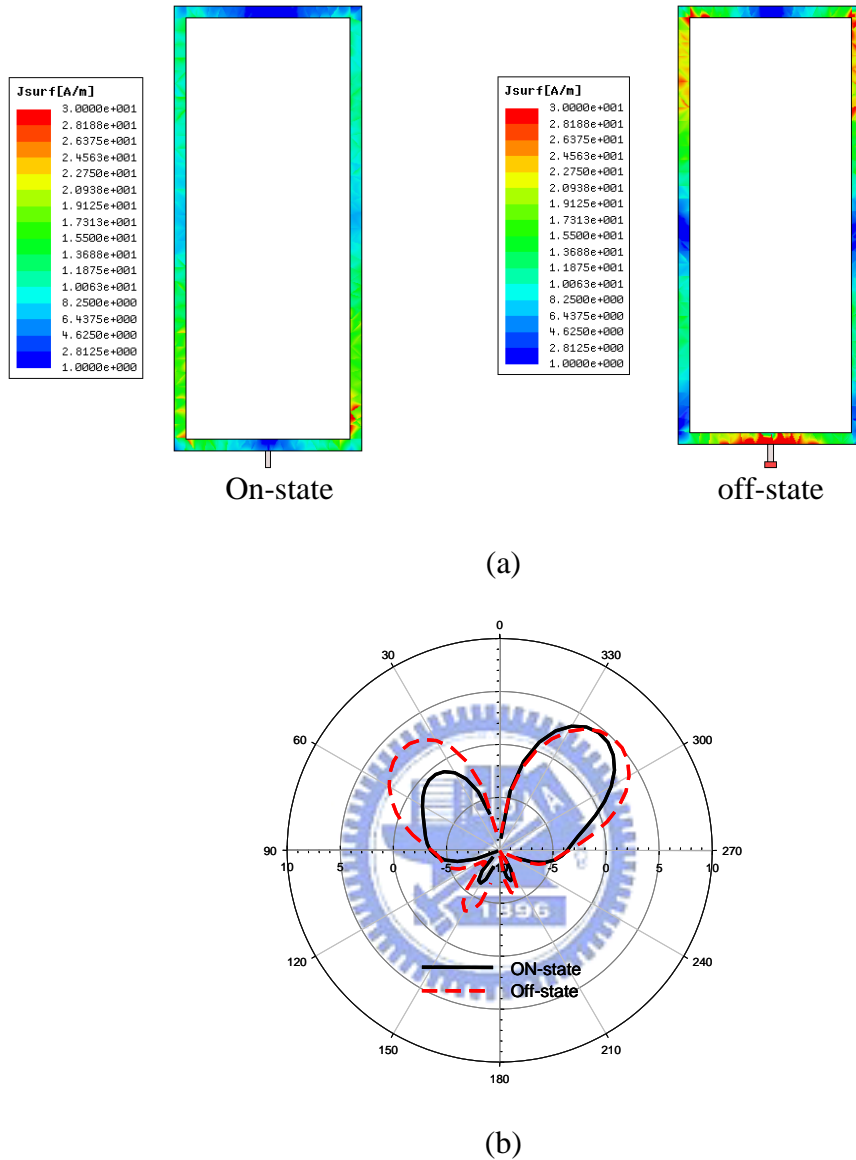


Fig. 5.7. The effects of the increment of the width, L_{lp} . (a) The current distribution on the loop in on- and off-state at 5.25 GHz. (b) The radiation patterns in on- and off-state at 5.25 GHz.

vertical arms affects the field, so the property of reflection is poor. As a result, a single loop with a dual-band reflection is developed.

If we increase the circumference of the loop, the reflection at 2.45 GHz can be improved, but the transmission at 5.25 GHz will be reduced due to the changes of current distribution of 5.25 GHz with the variation of the geometry. First, we increase the circumference by increasing the width, W_{lp} , to 20 mm. As shown in Fig. 5.6(a), the current distribution is similar to that of the original one when switch is impassable, so it

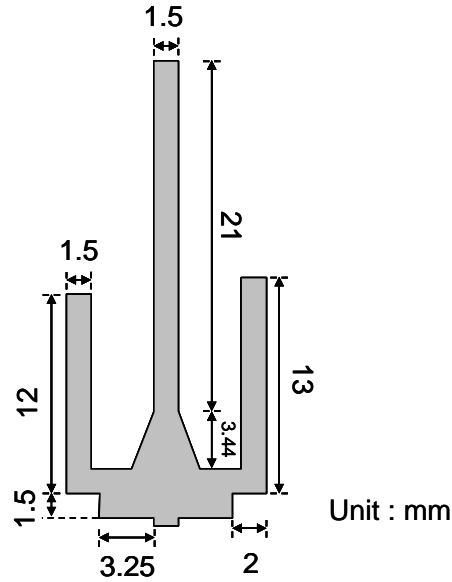


Fig. 5.8. The geometry of the center dual-band feeding antenna.

can reflect waves. Nevertheless, when the switch is passable, the resonant current distribution becomes five-quarter wavelength of 5.25 GHz. Even though one of the strong current which is on the bottom horizontal arm is cancelled by the ground, there are still two strong currents on each vertical arm. As a result, a good reflection remains, which means we cannot switch the reflector to be transparent to the incident waves. The simulated results of increasing the length, L_{lp} , to 38 mm are shown in Fig. 5.7. The reason that we cannot increase the length of the loop is the same as the reason for increment of the width. On the other hand, the current distributions at both states do not change significantly by a small variation of the dimensions of the loop. Therefore, the dimensions we design here are the best one to form a dual-band reflector with a single loop.

5-2-2 Design of the feeding antenna

As shown in Fig. 5.8, the center dual-band antenna is introduced. It is made of a piece of copper with conductivity of 5.8×10^7 S/m. The geometry of the antenna is a trident shape with unbalance arms at the both sides. The center arm resonates at 2.45 GHz while the unbalanced arms at the both sides are for 5.25 GHz. The dimensions of the antenna are in the figure. The taper structure is used to match the impedance, and the unbalance arms can increase the bandwidth at 5.25 GHz [27]. The simulated and measured results

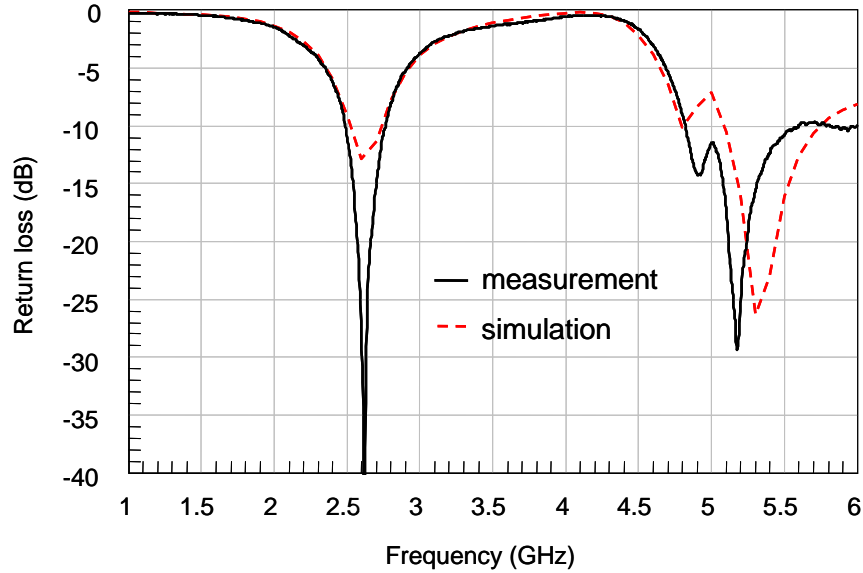


Fig. 5.9. The measured and simulated results of the center dual-band feeding antenna.

are shown in Fig. 5.9. The solid line is the measured result while the dash line is the simulated result. The measured result is similar to the simulated result: the impedance bandwidth under -10 dB is between 2.48 GHz and 2.77 GHz for the lower frequency band, and it is almost from 4.8 GHz to at least 6 GHz in according to the measured result. Even though the lower frequency band is a little higher here, the lower frequency band will move lower when the sidewalls are implemented.

5-3 MEASUREMENT RESULTS

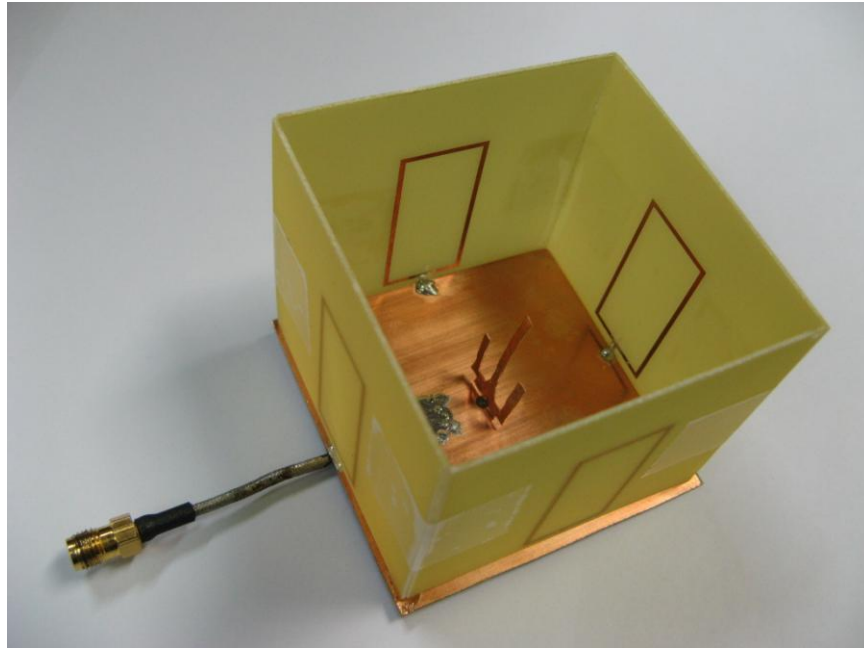


Fig. 5.10. The photo of the complete dual-band pattern reconfigurable antenna.

The complete dual-band pattern reconfigurable reflector antenna is shown in Fig. 5.10. We define the passable switch state as “on” while the impassable switch state as “off”. The simulated and measured results are listed in TABLE IV. In Case 1, all the switches are on. Therefore, waves can go through each wall unretardedly. The simulated and measured return losses in this case are shown in Fig. 5.11. The measured result coincide with the simulated one well. The impedance bandwidth under -10 dB is from 2.18 GHz to 2.6 GHz at the lower frequency band and from 5.04 GHz to 5.56 GHz at the higher frequency band. All of them are enough for use in our design. In Case 2, the switches, C and D, are on, while A and B are off. In this case, a corner reflector antenna is formed. Its simulated and measured results are shown in Fig. 5.12. There are resonances at both frequency bands of 2.55 GHz and 5.25 GHz, and the measured result is almost the same as the simulated one.

In Case 2, the directional patterns can be achieved, as shown in Fig. 5.13. The main beams indicate the direction of where the switches are on. The maximum gain of 4.19 dB appears at $\phi=225^\circ$, $\theta=-72^\circ$ at 2.55 GHz, and the maximum gain of 8.43 dB shows at $\phi=225^\circ$, $\theta=-48^\circ$ at 5.25 GHz. Besides, the front-to-back (FTB) ratio is an important

TABLE IV
 THE DEFINITIONS OF THE TWO FUNDAMENTAL CASES AND THE SIMULATED RESULTS OF
 THE DUAL-BAND PATTERN RECONFIGURABLE ANTENNA BY FOUR RECTANGULAR LOOPS

Switch		Case1	Case2
A		On	Off
B		On	Off
C		On	On
D		On	On
<i>Simulated peak gain direction</i>	2.55GHz	Omni	$\theta = -65^\circ$ $\phi = 225^\circ$
	5.25GHz	Omnilike	$\theta = -45^\circ$ $\phi = 225^\circ$
<i>Simulated peak gain (dBi)</i>	2.55GHz	2.18	4.83
	5.25GHz	4.75	8.76
<i>Measured peak gain direction</i>	2.55 GHz	Omni	$\theta = -72^\circ$ $\phi = 225^\circ$
	5.25 GHz	Omnilike	$\theta = -48^\circ$ $\phi = 225^\circ$
<i>Measured peak gain (dBi)</i>	2.55 GHz	1.57	4.19
	5.25 GHz	4.65	8.43

parameter for a directional antenna. The FTB ratio of 2.55 GHz is 4.92 dB, and that of 5.25 GHz is 13.47 dB, which can cancel the interferences from unwanted signals. Moreover, we can change our radiation patterns within four directions at dual frequencies by controlling the switch states. In Case 1, an omni-directional pattern is provided. In Fig. 5.14, the radiation patterns in xz- and yz-plane are shown. The gain of radiation patterns at the about angle of $\theta = 45^\circ$ at both frequencies, however, are close. Therefore, we can conclude omni-directional patterns in $\theta = 45^\circ$ plane. The measured maximum gain of

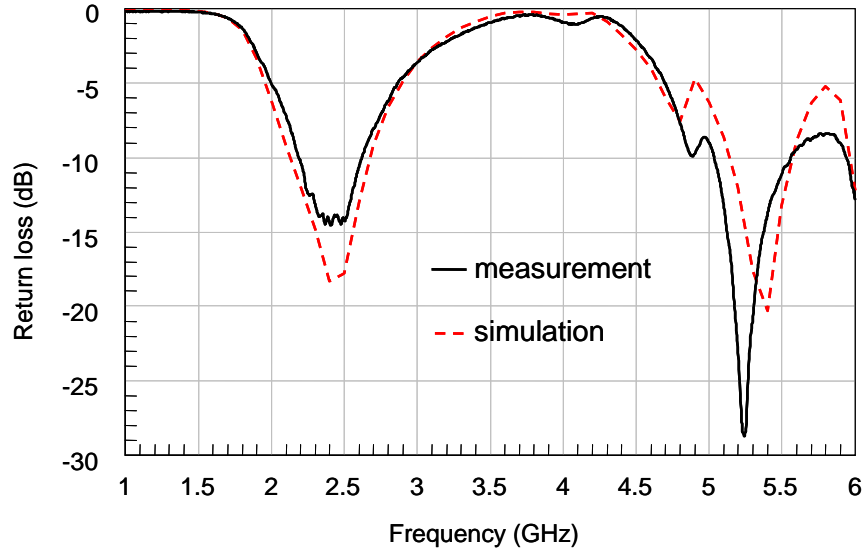


Fig. 5.11. The measured and simulated results of the return losses in Case 1.

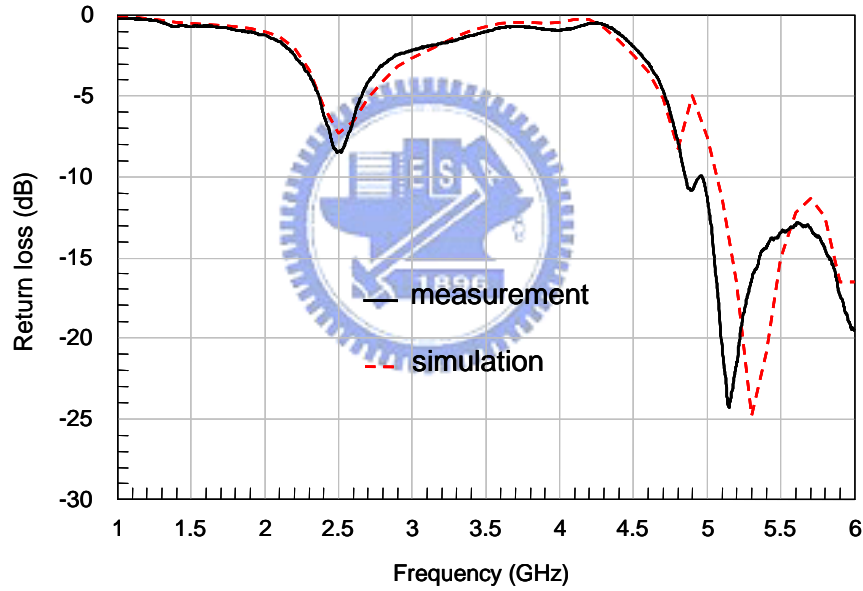
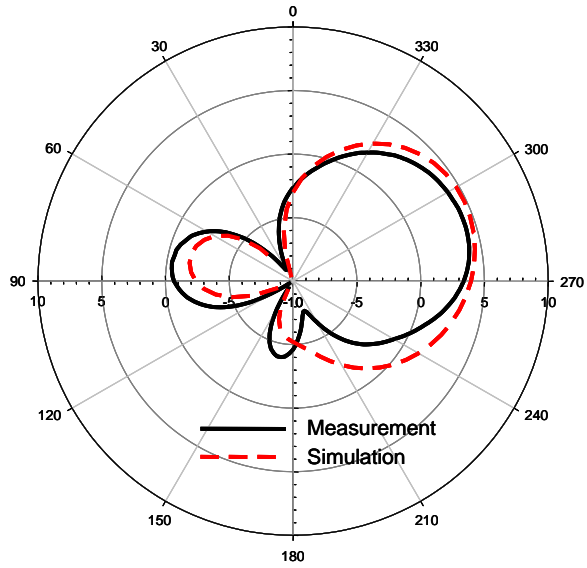
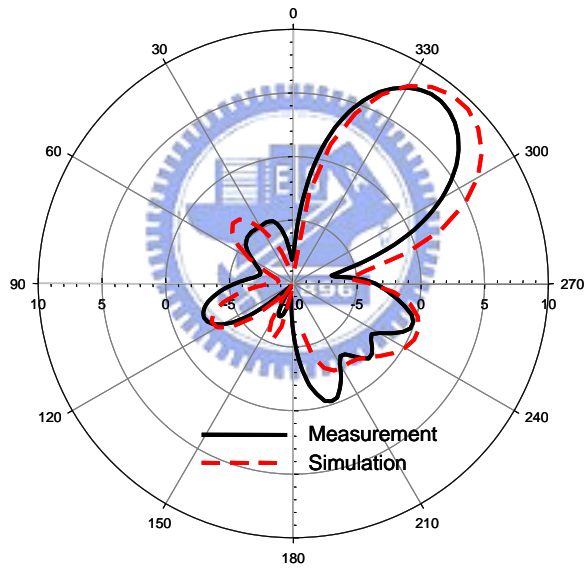


Fig. 5.12. The measured and simulated results of the return losses in Case 2.

2.45 GHz is 1.57 dB while that of 5.25 GHz is 4.65 dB. The differences of the maximum gains between the two cases are more than 3dB, so the variations of the patterns in different cases are apparent, which is good for real applications. The radiation patterns in xy-plane are not showing due to the ground effect which makes the patterns tilt.



(a)



(b)

Fig. 5.13. The measured and simulated radiation patterns in $\phi = 45^\circ$ -plane in Case 2 at (a) 2.55 GHz. (b) 5.25 GHz.

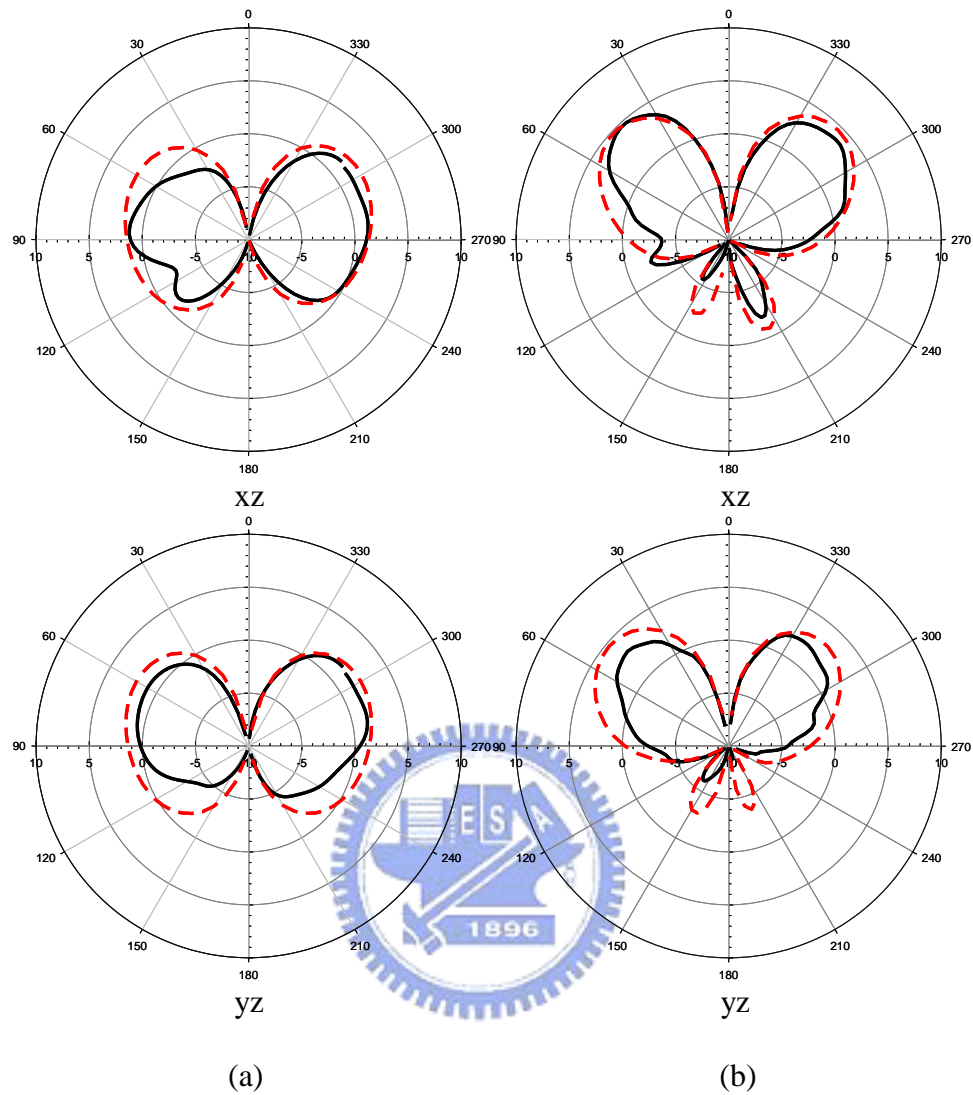


Fig. 5.14. The measured and simulated radiation patterns in xz - and yz -plane in Case 1 at (a) 2.55 GHz. (b) 5.25 GHz.

Chapter 6 CONCLUSION

In this thesis, three dual-band pattern reconfigurable antennas are presented. They all evolved from the corner reflector antenna. The design concept of the reflectors in every antenna is from the frequency selective surface. Due to changing the current distributions on the reflectors by switch states, the properties of transmission and reflection can be switched. The antennas presented here are dual-band, which has wider application nowadays. The first proposed antenna with two-layer walls has the omni-directional pattern at both frequencies and has the directional pattern with peak gain of 5.85 dBi at 2.45 GHz and 9.18 dBi at 5.25 GHz. The eight switches are needed here. Then, in the second proposed antenna, only one wall is used to reflect waves at both frequencies. Therefore, only one-layer walls are needed. The omni-directional patterns at both frequencies can be obtained, while the directional patterns with peak gain of 3.54 dBi at 2.55 GHz and 7.77 dBi at 5.25 GHz are measured. In addition, only four switches like DPDT are required to control the dual-band reflectors. In the end, a dual-band pattern reconfigurable antenna with four simple loops is investigated. The measured properties do not differentiate much from that of the second antenna. The maximum gain is 4.19 dBi at 2.55 GHz and 8.43 dBi at 5.25 GHz when a directional pattern is used. Omni-directional pattern can be achieved too. Besides, due to the simple structure, the switches we used and the associate circuitry become easier to fabricate. Therefore, it is good for application.

In conclusion, these three dual-band pattern reconfigurable antennas are good candidates for base station applications. All of them can operate in two frequency bands, and the patterns can be switched. Besides, because it is easy to fabricate and its design idea is simple, the other operating frequencies are easy to design. Therefore, the operating range can be easily changed.

REFERENCES

- [1] Wikipedia. Available: http://en.wikipedia.org/wiki/Smart_antenna
- [2] S. Zhang, G. H. Huff, J. Feng, and J. T. Bernhard, "A Pattern Reconfigurable Microstrip Parasitic Array," *IEEE Trans. Antennas Propagat.*, vol. 52, no. 10, pp. 2773-2776, Oct. 2004.
- [3] L. Petit, L. Dussopt, and J. M. Laheurte, "MEMS-Switched Parasitic-Antenna Array for Radiation Pattern Diversity," *IEEE Trans. Antennas Propagat.*, vol. 54, Issue 9, no. 6, pp. 2624-2631, Sep. 2006.
- [4] M. R. Kamarudin and P. S. Hall, "Disc-loaded Monopole Antenna Array for Switched Beam Control," *IEE Electronics Letters*, vol. 42, Issue 2, pp. 66-67, Jan. 2006.
- [5] H. M. Elkamchouchi and H. E. D. M. Hafez, "Switchable Beam Diversity Antenna," in *ICMMT*, Aug. 2002, pp. 377-380.
- [6] N. L. Scott, M. O. Leonard-Taylor, and R. G. Vaughan, "Diversity Gain from a Single-Port Adaptive Antenna Using Switched Parasitic Elements Illustrated with a Wire and Monopole Prototype," *IEEE Trans. Antennas Propagat.*, vol. 47, no. 6, pp. 1066-1070, June 1999.
- [7] J.W. Lu, D.V. Thiel, B. Hanna, and S. Saario, "Multi-beam Switched Parasitic Antenna Embedded in Dielectric for Wireless Communications Systems," *IEE Electronics Letters*, vol. 37, no. 14, pp. 871-872, July 2001.
- [8] S. Preston and D. V. Thiel, "Direction Finding Using A Switched Parasitic Antenna Array," in *IEEE AP-S Int. Symp.*, July 1997, vol. 2, pp. 1024-1027.
- [9] S. S. L. Yang and K. M. Luk, "A Wideband L-probe Fed Patch Antenna for Pattern Reconfiguration," in *IEEE AP-S Int. Symp.*, vol. 2B, pp. 581-584, July 2005.
- [10] M. D. Migliore, D. Pinchera, and F. Schettino, "A Simple and Robust Adaptive Parasitic Antenna," *IEEE Trans. Antennas Propagat.*, vol. 53, no. 10, pp. 3262-3272, Oct. 2005.
- [11] Robert Schlub and David V. Thiel, "Switched Parasitic Antenna on a Finite Ground Plane With Conductive Sleeve," *IEEE Trans. Antennas Propagat.*, vol. 52, no. 5, pp. 1343-1347, May 2004.

- [12] Y. Nakane, T. Noguchi, and Y. Kuwahara, "Trial Model of Adaptive Antenna Equipped with Switched Loads on Parasitic Elements," *IEEE Trans. Antennas Propagat.*, vol. 53, no. 10, Oct. 2005.
- [13] L. Low and R.J. Langley, "Single Feed Antenna with Radiation Pattern Diversity," *IEE Electronic Letters*, vol. 40, no. 16, pp. 975-976, Aug. 2004.
- [14] R. Vaughan, "Switched Parasitic Elements for Antenna Diversity," *IEEE Trans. Antennas Propagat.*, vol. 47, no. 2, pp. 399-405, Feb. 1999.
- [15] W. L. Stutzman and G. A. Thiele, *Antenna Theory and Design*. New York: Wiley & Sons Inc., 1997.
- [16] N. Inagaki, "Three-Dimensional Corner Reflector Antenna," *IEEE Trans. Antennas Propagat.*, vol. 22, iss. 4, pp. 580-582, July 1974.
- [17] N. Inagaki, K. Uchikawa, Y. Hashimoto, and N. Kikuma, "3-D Corner Reflector Antenna and its Analysis using UTD," in *IEEE AP-S Int. Symp.*, June 1994, pp. 598-601.
- [18] K.T. Mathew, J. Jacob, S. Mathew, and U. Raveendranath, "Triple Corner Reflector Antenna and Its Performance in H-plane," *IEE Electronic Letters*, vol. 32, no. 16, pp. 1432, Aug. 1996.
- [19] H. M. Elkamchouchi, "Cylindrical and Three-Dimensional Corner Reflector Antennas," *IEEE Trans. Antennas Propagat.*, vol. AP-31, no. 3, pp. 451-455, May 1983.
- [20] J. C. Ke, C. W. Ling, and S. J. Chung, "Implementation of a Multi-Beam Switched Parasitic Antenna for wireless applications," in *IEEE AP-S Int. Symp.*, July 2007, pp. 3368-3371.
- [21] R. Remski, B. Gray, and L. Ma, "Frequency Selective Surfaces - Design and Analysis using the Ansoft Product Suite".
- [22] B. Hooberman, "Everything You Ever Wanted to Know About Frequency-Selective Surface Filters but Were Afraid to Ask," May 2005.
- [23] D. H. Kim and J. I. Choi, "Design of a Multiband Frequency Selective Surface," *ETRI Journal*, vol. 28, no. 4, Aug. 2006.
- [24] J. Romeu and Y. Rahmat-Samii, "A Fractal Based FSS with Dual Band Characteristics," in *IEEE AP-S Int. Symp.*, vol. 3, pp. 1734-1737, Aug. 1999.

- [25] D. M. Pozar, Microwave Engineering, 3rd ed. New York: Wiley, 2005.
- [26] HFSS, Ansoft Corporation, Pittsburgh, PA.
- [27] M.J. Ammann and R. Farrell, “Dual-band Monopole Antenna with Stagger-tuned Arms for Broadbanding,” in IEEE IWAT, Mar. 2005, pp. 278-281.

